Bridging the spatial gaps of the Ammonia Monitoring Network using satellite ammonia measurements

Rui Wang[1], Da Pan[1], Xuehui Guo[1], Kang Sun[2,3], Lieven Clarisse[4], Martin Van Damme[4,5], Pierre-François Coheur[4], Cathy Clerbaux[4,5,6], Melissa Puchalski[7], and Mark A. Zondlo[1*]

[1]Department of Civil and Environmental Engineering, Princeton University, Princeton, NJ, USA
[2]Department of Civil, Structural and Environmental Engineering, University at Buffalo, Buffalo, NY, USA
[3]Research and Education in eNergy, Environment and Water (RENEW) Institute, University at Buffalo, Buffalo, NY, USA
[4]Université libre de Bruxelles (ULB), Spectroscopy, Quantum Chemistry and Atmospheric Remote Sensing (SQUARES), Brussels, Belgium
[5]Royal Belgian Institute for Space Aeronomy, Brussels, Belgium
[6]LATMOS/IPSL, Sorbonne Université, UVSQ, CNRS, Paris, France
[7]Office of Air and Radiation, US Environmental Protection Agency, Washington, DC, USA

Correspondence to: Mark A. Zondlo (mzondlo@princeton.edu)

Abstract. Ammonia (NH_3) is a key precursor to fine particulate matter ($PM_{2.5}$) and a primary form of reactive nitrogen. The limited number ~~observations~~ of NH_3 observations hinders further understanding of its impacts on air quality, climate, and biodiversity. Currently, NH_3 ground monitoring networks are ~~limited in number~~few and sparse across most of the globe, and even in the most established networks, large spatial gaps exist between sites and only a few sites have records that span longer than a decade. Satellite NH_3 observations can be used to discern trends and fill spatial gaps in networks, but many factors influence the syntheses of the vastly different spatiotemporal scales between surface network and satellite measurements. To this end, we intercompared surface NH_3 data from the Ammonia Monitoring Network (AMoN) and satellite NH_3 total columns from the Infrared Atmospheric Sounding Interferometer (IASI) in the contiguous United States (CONUS) and then performed trend analyses using both datasets. We explored the sensitivity of correlations between the two datasets to factors such as satellite data availability and distribution over the surface measurement period as well as agreement within selected spatial and temporal windows. Given the short lifetime of atmospheric ammonia and consequently sharp gradients, smaller spatial windows show better agreement than larger ones except in areas of relatively uniform, low concentrations where large windows and more satellite measurements improve the signal-to-noise ratio. A critical factor in the comparison is having satellite measurements across most of the measurement period of the monitoring site. When IASI data are available for at least 80% days of AMoN's 2-week sampling period within a 25 km spatial window of a given site, IASI NH_3 column concentrations and the AMoN NH_3 surface concentrations have a correlation of 0.74, demonstrating the feasibility of using satellite NH_3 columns to bridge the spatial gaps existing in the surface network NH_3 concentrations. Both IASI and AMoN show increasing NH_3 concentrations across CONUS (median: $6.8\% \cdot yr^{-1}$ vs. $6.7\% \cdot yr^{-1}$) in the last decade (2008 - 2018), ~~stressing the rising~~suggesting

the ~~importance of~~ NH$_3$ will become a greater contributor to~~in terms of~~ nitrogen deposition. NH$_3$ trends at AMoN sites are correlated with IASI NH$_3$ trends (r = 0.66), and show similar spatial patterns, with the highest increases in the Midwest and eastern U.S.~~NH$_3$ trends for AMoN sites correlates with IASI NH$_3$ trend IASI and AMoN NH$_3$ trend (r = 0.66) and show a similar spatial pattern, with the highest increases in the Midwest and eastern U.S., and NH$_3$ trend for AMoN sites correlates with IASI NH$_3$ trend (r = 0.66).~~ In spring and summer, increases of NH$_3$ were larger than 10%·yr^{-1} in the eastern U.S. and Midwest (cropland dominated) and ~~the~~ western U.S. (pastureland dominated), respectively. ~~In terms of trend in~~ NH$_3$ hotpots (defined as regions where the IASI NH$_3$ column is larger than the 95th percentile of 11-year CONUS map, 6.7 × 10^{15} molec/cm^2), ~~these largest emissions sources are~~ also experiencing increasing concentrations over time, with a~~the~~ median of NH$_3$ trend ~~of~~is 4.7% · yr^{-1}. IASI data show large NH$_3$ increases in urban areas (8.1%·yr^{-1}), including 8 of the top 10 most populous regions in the CONUS, where AMoN sites are sparse. A comparison between IASI NH$_3$ concentration trends and state-level NH$_3$ emission trends is then performed to reveal that positive correlations exist in states with strong agricultural NH$_3$ emissions while negative correlations in states with low NH$_3$ emissions and large NO$_x$ emissions, suggesting the different roles of emission and partitioning in NH$_3$ increases. The increas~~ing~~e in NH$_3$ could have detrimental effects on nearby eco-sensitive regions through nitrogen deposition and on aerosol chemistry in the densely populated urban areas, and therefore should be carefully monitored and studied.~~hence needs immediate attention.~~

1 Introduction

Gas phase ammonia (NH$_3$) is the most abundant alkaline gas in the atmosphere, mainly emitted from agricultural activities such as nitrogen fertilizer applications and livestock waste volatilization (Bouwman et al., 1997; Paulot et al., 2014). As a major precursor to fine particulate matter (PM$_{2.5}$), NH$_3$ critically affects aerosol heterogeneous chemistry, air quality, visibility, human health, and climate (Hauglustaine et al., 2014; Hill et al., 2019; Lawal et al., 2018; Malm et al., 2004). Ammonia neutralizes sulfuric acid (H$_2$SO$_4$) and nitric acid (HNO$_3$) in the atmosphere to form ammoniated aerosols, ammonium sulfate ((NH$_4$)$_2$SO$_4$) and ammonium nitrate (NH$_4$NO$_3$), which in total can contribute to more than 50 % of total PM$_{2.5}$ mass (Feng et al., 2020). NH$_4$NO$_3$ is critical during wintertime haze periods because the cold and humid condition favor its formation (Shah et al., 2018; Zhai et al., 2021). Besides, NH$_3$ plays an important role in the nitrogen cycle. Wet deposition of NH$_4^+$ dominates the wet inorganic nitrogen deposition at nearly 70% of monitoring sites in the United States (Li et al., 2016). Total NH$_x$ (≡NH$_3$(g) + NH$_4^+$ (aq)) deposition is expected to become even more dominant in the future because NO$_x$ emissions are decreas~~ing~~e under new pollution control~~s~~ while NH$_3$ emissions are predicted to continue to increase with the rising global food demands (Erisman et al., 2008; Goldberg et al., 2021; Pinder et al., 2008). Excessive NH$_3$ deposition in the non-agricultural ecosystems can reduce biodiversity, result in soil acidification, and increase eutrophication, especially in ~~the~~ sensitive ecosystems (Ellis et al., 2013; Phoenix et al., 2006).

65   Although NH$_3$'s importance has been well recognized, routine NH$_3$ observations are lacking even in countries with comprehensive monitoring networks, partly due to the difficulty of measuring gas phase NH$_3$ (von Bobrutzki et al., 2010; Fehsenfeld et al., 2002). The Ammonia Monitoring Network (AMoN) (Puchalski et al., 2015) is the only routine set of NH$_3$ measurements in the United States, with 110 active AMoN sites in the contiguous United States (CONUS) in 2021, providing high-quality surface observations of NH$_3$. AMoN data have been used widely for model evaluation and long-term trend

70   analysis (Butler et al., 2016; Nair et al., 2019; Yao and Zhang, 2016, 2019). AMoN only provides bi-weekly NH$_3$ observations, in contrast to monitoring networks for two other important gas phase precursors of PM$_{2.5}$, SO$_2$ and NO$_2$, which provide hourly or daily scale observations. PM$_{2.5}$, SO$_2$, and NO$_2$ are directly regulated as criteria pollutants, however contributions from NH$_3$ emissions sources must be considered in State Implementation Plan (SIP) demonstrations for areas out of attainment for PM$_{2.5}$, which can be a challenge for areas lacking NH$_3$ measurements (EPA 2023).

75

Population weighted PM$_{2.5}$ concentrations are widely used to estimate the health effects of PM$_{2.5}$, however, the sparse number of NH$_3$ sites with only biweekly or monthly resolution makes it difficult to derive population weighted PM$_{2.5}$ precursor datasets. Gas phase NH$_3$ is critical to determine the partitioning of the total NH$_x$ (Hennigan et al., 2015), and the lack of gas phase NH$_3$ observations hampers the evaluation of chemistry models. The ISORROPIA-II thermodynamic model has been extensively

80   adopted to compute the equilibrium composition for the inorganic aerosol systems (Fountoukis and Nenes, 2007) and requires both gas and aerosol phase data as input to provide accurate and robust results (Hennigan et al., 2015). However, the limited number of NH$_3$ ground monitoring sites currently prevents synthesizing the AMoN NH$_3$ data with other ground monitoring networks, e.g., the Interagency Monitoring of Protected Visual Environments (IMPROVE)~~IMPROVE~~, as input for ISORROPIAII (Pan et al., 2020). GEOS-Chem implemented with ISORROPIA-II was found to significantly underestimate

85   gas phase NH$_3$ and overestimate NH$_4^+$ in winter (Holt et al., 2015; Nair et al., 2019; Walker et al., 2012), with the normalized NH$_4^+$ mean biases as high as 86% in January at sites for IMPROVE ~~the Interagency Monitoring of Protected Visual Environments (IMPROVE)~~ (Holt et al., 2015). The lifetime of NH$_3$ ranges from hours to days, hence large spatiotemporal variability exists (Golston et al., 2020; Miller et al., 2015; Wang et al.; 2021), and large spatial gaps exist in the current AMoN. Currently there are no AMoN sites in some states, e.g., North Dakota and South Dakota, and only 12 sites are within the

90   characteristic length scale (12 km) of NH$_3$ hotspot~~s~~ regions (Wang et al., 2021). Ten national parks in the U.S. are within 100 km of an NH$_3$ hotspot, and more observations are needed to quantify the impacts of these hotspots on dry NH$_3$ deposition in these regions (Pan et al., 2021). A lack of long-term AMoN data also hinders the possibility of investigating NH$_3$ trends in the CONUS. Increasing NH$_3$ concentrations are observed using AMoN data, yet all of the previous trend analyses are limited to fewer than 20 AMoN sites that may not be representative of NH$_3$ trends in the CONUS (Butler et al., 2016; Yao and Zhang,

95   2016, 2019).

Satellite NH$_3$ observations are on a global and daily basis, providing long-term trends and ubiquitous coverage. Instruments that measures NH$_3$ include the Infrared Atmospheric Sounding Interferometer (IASI) on the MetOp satellites, Cross-track

Infrared Sounder (CrIS) on NOAA and NASA Suomi National Polar-orbiting Partnership (S-NPP) and on Joint Polar Satellite
System-1 and -2 (JPSS-1 and -2), Tropospheric Emission Spectrometer (TES) on NASA Aura satellite, Atmospheric Infrared
Sounder (AIRS) on NASA EOS Aqua satellite, and Thermal and Near Infrared Sensor for Carbon Observations – Fourier
Transform Spectrometer (TANSO-FTS) on the Greenhouse Gases Observing SATellite (GOSAT) (Clarisse et al., 2009;
Shephard et al., 2011; Shephard & Cady-Pereira, 2015; Someya et al., 2020; Warner et al., 2016). Satellite NH_3 data have been
widely used to constrain NH_3 emissions, estimate NH_3 deposition, and analyze NH_3 trends (Cao et al., 2020; Chen et al., 2020;
Kharol et al., 2018; Van Damme et al., 2021). Van Damme et al. (2021) utilized 11-year IASI NH_3 observations a and found
a worldwide NH_3 increase (12.8 ± 1.3 %) from 2008 to 2018 with especially large increases in east Asia (75.7 ± 6.3 %) and
North America (26.8 ± 4.5 %). Warner et al. (2017) used 14-year AIRS NH_3 measurements and found statistically significant
NH_3 increase ($2.61\% \cdot yr^{-1}$) in the U.S. from 2002 to 2016.

The global daily coverage and long-term data record make it possible for satellite observations to fill the spatial and temporal
gaps of the current ground monitoring networks. Although limited in numbers, the validations of satellite NH_3 observations
with in-situ measurements provide confidence in integrating the two datasets (Guo et al., 2021; Sun et al., 2015). Sun et al.
(2015) performed the first daily and pixel scale satellite NH_3 validations using TES NH_3 columns and airborne NH_3
observations in the San Joaquin Valley of California, USA, showing that the differences between the total NH_3 column and
the in-situ total column were within 6 %. However, the validation included only 9 TES pixels, and TES is no longer in operation
now. Guo et al. (2021) showed that IASI NH_3 columns and NH_3 columns derived from airborne and ground-based NH_3
observations were indistinguishable from one another on daily and pixel bases in Colorado, USA, in summer. All of these
validation works were ~~performed~~ carried out in ~~certain~~ specific seasons and were limited to source regions with high NH_3
concentrations (Guo et al., 2021; Sun et al., 2015; Warner et al., 2016). Ground-based FTIR NH_3 observations provided a
better temporal coverage for evaluating IASI and CrIS NH_3 retrievals, however, low concentration sites were excluded from
the evaluation and only ~ 10 sites were included across the globe (Dammers et al., 2016; Dammers et al., 2017). Furthermore,
FTIR-based measurements also have not been directly validated against in-situ measurements of NH_3 vertical profile
themselves.

To capitalize on the benefits of both surface and satellite observations and synthesize these datasets, a detailed understanding
of the comparison between IASI NH_3 column concentrations and AMoN NH_3 surface concentrations is necessary. Here we
focus on IASI NH_3 measurements because it offers the longest data record (2008 - present) among the satellite NH_3-measuring
instruments. The comparison between AMoN and IASI is complex because AMoN is a ground-based, point measurement
integrated over fourteen days, whereas IASI is a space-borne volumetric measurement averaged over the pixel footprint at the
instantaneous overpass time. There are several factors that need to be taken into consideration:

(1) The extent to which the IASI NH$_3$ column represents the surface AMoN NH$_3$ concentration: Knowledge of NH$_3$ vertical profiles in the atmosphere ~~are~~ is limited due to the lack of observational data, and model simulated NH$_3$ vertical profiles are often biased compared with the airborne measurements (Schiferl et al., 2016). Ammonia is mostly concentrated in the planetary boundary layer (PBL) because of its short lifetime (~hours to days) and surface emission sources (Dentener & Crutzen, 1994; Guo et al., 2021; Sun et al., 2015; Seinfeld & Pandis, 2016). Sun et al. (2015) showed that NH$_3$ was almost well mixed in the lower PBL, and the TES NH$_3$ columns were strongly correlated (R^2 = 0.82) with the median NH$_3$ mixing ratios measured at the surface, demonstrating that satellite NH$_3$ columns could represent the ground NH$_3$ concentrations. Van Damme et al. (2015) converted IASI NH$_3$ columns to surface NH$_3$ concentrations using fixed NH$_3$ profiles generated by GEOS-Chem, then performed monthly comparisons with ground monitoring networks. IASI derived surface NH$_3$ observations are in fair agreement with ground observations in Europe, China, and Africa, but are limited to a small number of sites in each region for a short time range, e.g., 27 sites in Europe in 2011 (Van Damme et al., 2015). Furthermore, the latest IASI NH$_3$ products have switched to a new algorithm and no longer use a fixed NH$_3$ profile (Whitburn et al., 2016; Van Damme et al., 2017).

(2) Optimal spatial window for comparing and integrating satellite pixels and AMoN sites: Previous comparisons of satellite NH$_3$ retrievals with observations from ground monitoring networks simply averaged the data from the monitoring site within a coarse model grid (~ 100 km) with the averaged modeling/satellite NH$_3$ concentration of the whole grid (Kharol et al., 2018; Nair et al., 2019; Van Damme et al., 2015). If NH$_3$ concentrations are uniformly distributed within the spatial window, increasing the spatial window will increase the number of IASI pixels and decrease the signal-to-noise ratio. However, the spatial heterogeneity of NH$_3$ is quite large near hotspots due to its short lifetime (Golston et al., 2020; Miller et al., 2015; Wang et al., 2021; Warner et al., 2016). The relationship between spatial window size and satellite/surface measurements agreement needs to be examined in more detail~~s~~.

(3) Temporal distribution of satellite measurements across the two-week AMoN sampling period: Previous comparisons of model or satellite products against surface observations did not consider the distribution of IASI measurements during the two-week sampling period (Kharol et al., 2018; Nair et al., 2019; Van Damme et al., 2015). AMoN measures continuously, whereas a series of cloudy days would preclude any valid satellite measurements. Therefore, any AMoN/satellite comparison is intrinsically biased towards clear sky days on the satellite side but includes all conditions for the AMoN site.

(4) Number of available IASI pixels in the comparison: Guo et al. (2021) has shown that, even at low column amounts, IASI NH$_3$ has no known biases. AMoN is an extremely sensitive measurement of NH$_3$, far more precise than any satellite NH$_3$ product (NADP, 2023; Van Damme et al., 2017). Therefore, increasing the number of satellite measurements within a certain spatiotemporal window is expected to improve the signal-to-noise ratio in the satellite measurements and may lead to improved agreements with AMoN under clean conditions.

(5) Regional and seasonal variabilities: Different regional and seasonal patterns are expected to influence the comparison. The performances of thermal infrared sounders are highly affected by the thermal contrast between the surface air temperature and skin temperature (Clarisse et al., 2010). In winter, low thermal contrast results in low sensitivity, which explains the low number of IASI pixels in winter compared to summer (Clarisse et al., 2010; Guo et al., 2021). Kharol et al. (2018) showed that CrIS surface NH$_3$ concentrations had an overall mean CrIS–AMoN difference of ∼+15%, however, they only averaged CrIS data over the warm season in 2013.

In this study, to demonstrate the capabilities of using IASI NH$_3$ observations to augment the ground monitoring network, we performed a comprehensive comparison between IASI and AMoN on bi-weekly/seasonal scales. We directly compare the correlation between IASI NH$_3$ columns with AMoN surface NH$_3$. We avoided ~~direct comparisons when~~ converting column NH$_3$ into surface concentrations because of possible biases introduced by assuming vertical profiles, boundary layer heights at local sites, and gas phase - aerosol partitioning. The impacts of the different factors on the comparison are examined in the context of points raised above. After identifying the most optimal method for comparison, we examined NH$_3$ trends over AMoN sites and the larger applicability of using satellite retrievals to discern NH$_3$ trends over regions and seasons lacking AMoN data.

2 Data and methods

2.1 Satellite NH$_3$ observations

IASI is an infrared sounder ~~launched~~deployed on board of the MetOp-A, MetOp-B, and MetOp-C platforms in sun-synchronous orbits since October 2006, September 2012, and November 2018, respectively. IASI has a swath of 2200 km and provides global coverage twice per day at around 09:30 and 21:30 mean local solar time. At nadir, the IASI footprint has a 12-km diameter. The first IASI NH$_3$ product was developed by Clarisse et al. (2009) by converting the brightness temperature differences into total NH$_3$ columns. Later on, a flexible and robust retrieval algorithm based on an artificial neural network for IASI (ANNI) (Whitburn et al., 2016) was developed. The latest version ~~consists of~~is a reanalyzed dataset ~~provided with~~that uses the European Centre for Medium-Range Weather Forecasts Re-Analysis v5 (ERA5) as its meteorological input (Van Damme et al., 2017; Van Damme et al., 2021). Because the~~se~~ meteorological ~~input~~ data ~~for reanalysis data is~~are coherent in time, the reanalysis dataset it is the mo~~re~~st appropriate dataset ~~to be used~~ to study trends. For the present analyses, we used IASI version 3.1 reanalysis (v3.1r) retrieval product data from the MetOp/A (2008-2018) and MetOp/B (2013-2018) satellites (limited to cloud fraction ≤ 25 %). Only the morning orbits were analyzed because of higher sensitivity than the evening overpasses (Clarisse et al., 2010).

2.2 Ground-based observations

AMoN is the only network providing a consistent, long-term record of NH_3 gas concentrations across the United States. AMoN was established by the National Atmospheric Deposition Program (NADP) in October 2007 and expanded to 19 sites in 2010 and 105 sites in 2018. AMoN deploys Radiello® passive samplers that rely upon diffusion theory, where gas phase NH_3 is adsorbed onto a cylindrical interior filter and extracted as NH_4^+ to be analyzed by Flow Injection Analysis (FIA). AMoN provides biweekly surface NH_3 concentrations, and the network detection limit is 0.083 mg NH_4^+ L^{-1} (~0.078 µg NH_3 m^{-3}) for the 2-week samples in 2020 (NADP, 2023). The Radiello passive samplers were found to be biased low by 37% against denuders used as reference method (Puchalski et al., 2011). In this study, we are comparing the relative variations instead of absolute concentrations of IASI and AMoN, therefore the low bias of AMoN measurements is not as relevant to the outcome.

We incorporated data from all AMoN sites with one notable exception. Using satellite imagery, we ~~identified~~ determined that the AMoN site in Logan, Utah (UT01), is located only ~ 100 m away from a livestock farm. Ammonia concentrations downwind of a beef/dairy feedlot at this distance are far above background levels and unrepresentative of those at the local-regional scales (1-10 km) (Golston et al., 2020; Miller et al., 2015; Sun et al., 2018). Concentrations at UT01 are expected to be strongly dependent upon the extent to which local winds blow directly from that farm to the AMoN site throughout the two-week integration period. Not surprisingly, the UT01 site has the highest annual mean concentration (16.2 µg/m^3) in the entire AMoN network (three times higher than the next one). Furthermore, this AMoN site may be particularly susceptible to trends in animal operations or management practices at the farm. While it is possible the measurements of UT01 are representative of the local region, it is beyond the scope of this work to make such an assessment of its representativeness. For trend analyses, we only include AMoN sites with full year coverage during 2008 - 2018 (N=13).

2.3 Trend analyses

2.3.1 Oversampled NH_3 maps for trend analysis

From 2008 to 2018, a 0.02° × 0.02° (~2 km) annual mean NH_3 map in the CONUS was created each year based on a physical oversampling algorithm that represents the satellite spatial response functions as generalized 2-D super Gaussian functions (Sun et al., 2018). This algorithm weighs IASI measurements by their uncertainties, which include varying sensitivities to thermal contrast as described in Sun et al. (2018) and Wang et al. (2021). To evaluate the seasonal trends, ~~F~~for each year, seasonally averaged oversampling maps were also generated for spring (March, April, and May, MAM), summer (June, July, and August, JJA), fall (September, October, and November, SON), and winter (December, January, and February, DJF). For each season, we were able to achieve sufficiently overlapped IASI pixels through calculating the sum of the unnormalized spatial response function (SRF) of the oversampling results. A large sum of unnormalized SRF means the Level 3 grid is

covered by more Level 2 pixels. (Sun et al., 2018 and, Wang et al., 2021 have a detailed description of SRF.). The oversampling products are only used for the trend analyses in Section 4 to achieve a high spatial resolution. For IASI and AMoN comparison results in Section 3, the oversampling products are not used since it sacrifices the temporal resolution.

2.3.2 Mann-Kendall test and Theil-Sen's slope estimator for trend analysis

We use the Mann-Kendall (MK) test and Theil-Sen's slope estimator for NH_3 trend analyses. The non-parametric Mann-Kendall test and Theil-Sen's slope estimator are widely used in detecting trends of variables in meteorology and hydrology fields (Ahn and Merwade, 2014; Kendall, 1975; Yue and Wang, 2004). The Kendall rank correlation coefficient, commonly referred to as Kendall's τ coefficient, is a statistic used to measure the rank correlation. An MK test is a non-parametric hypothesis test for statistical dependence based on the Kendall's τ coefficient. The Theil–Sen's slope estimator is commonly used to fit a line to data points by calculating the median of the slopes of all lines through pairs of points.

Different fromUnlike simple linear regression, the Mann-Kendall test and Theil-Sen's slope estimator do not require the data to follow normal distribution and therefore are more robust to any outliers (Yue and Wang, 2004). This method is computationally efficient and is insensitive to outliers. For skewed and heteroskedastic data, the Theil-Sen estimator can be significantly more accurate than linear least squares regression. For normally distributed data, the Theil-Sen estimator competes well against the least squares in terms of statistical power (Yue and Wang, 2004).

In this study, Theil-Sen's slope was used to estimate 2008 – 2018 NH_3 trends, and the MK test was used to derive the significance level of trends.

3 IASI & AMoN comparison

3.1 Sensitivity to spatial windows

For the initial analysis, we first usedshow the simplest way ofmethod for comparing the satellite measurements with ground observations. In other words, for we center on each AMoN site, we average all IASI observations within a given radius of the AMoN site for during the sampling time frame (2 weeks) for comparison, and refer to that radius as a spatial window. We define each AMoN sample with co-located IASI pixels as an AMoN-IASI pair. If the distribution of NH_3 pixels is spatially uniform, increasing the spatial window may improve the correlation between the two datasets because of a larger number of IASI pixels. Larger spatial windows include more IASI pixels than smaller spatial windows but at the expense of potentially not being representative of the AMoN site. In addition, a larger region is likely to encompass NH_3 spatial gradients. In contrast, small spatial windows may only include a limited number of IASI pixels, encompassing more inherent

260 noise in the satellite measurements, especially if close to the detection limit. Each integrated 2-week AMoN measurement for each site was correlated with any relevant satellite data within the spatial window (total of 104 AMoN sites with 16,093 measurements). Correlations between IASI and AMoN for different spatial windows (15 km, 25 km, 50 km, and 100 km) are summarized in Table 1. The minimum spatial window radius of 15 km is based upon an approximate scale for NH_3 hotspots (Wang et al. 2021).

265

As the spatial window becomes larger, mean temporal coverage (defined as the percentage of days with available IASI data of the 2-week AMoN sampling period) and the number of IASI pixels both have significant increases, but the Pearson's r coefficient only increases slightly from 0.35 at a 15 km spatial window to 0.44 at a 100 km spatial window. Indeed, doubling the spatial window from 50 km to 100 km yields an almost tripled mean number of IASI pixels, yet maintains the almost the
270 same correlation with r = 0.45 and r = 0. 44, respectively. This indicates that including IASI pixels at longer distances from the AMoN site may not be representative of the AMoN site, especially near sources or in regions with complex topography. The slightly increased r value over spatial window range may result from a tradeoff between averaging spatial gradients versus integrating a larger number of IASI pixels to improve the signal-to-noise ratio of the satellite measurements. To balance these competing effects, we select 25 km as the nominal spatial window for the further comparisons.

275

Table 1. AMoN & IASI comparison results for different spatial windows

Spatial window	15 km	25 km	50 km	100 km
Pearson's r	0.35	0.41	0.45	0.44
Mean temporal coverage per pair (%)	31	44	57	71
Mean # IASI pixels per AMoN-IASI pair	7	17	69	278
# AMoN-&-IASI pairs	14734	15543	15933	16022

3.2 Sensitivities to temporal coverage and the number of IASI pixels

NH_3 is a short-lived species with a complicated diurnal profile (Nair and Yu, 2020) and the potential for large day-to-day
280 concentration changes because of the variability in emissions, wind speed, temperature, PBL height, and aerosol partitioning (Golston et al., 2020; Miller et al., 2015). Thus, the temporal distribution of satellite measurements within the AMoN measurement period may impact the comparison. Fig. 1 illustrates four examples where the number of IASI pixels, and their relative distribution throughout the 2-week AMoN integration period (using a 25 km spatial window), could affect may impact

the resultscomparison (25 km spatial window). An ideal comparison case would have a uniform number of IASI measurements

285   on each day during the approximate 14-day AMoN measurement period, similar to the case shown in Fig. 1a. In this case, there is no specific day having more weight than the other when calculating the biweekly mean. More common, however, are cases where some days have no satellite measurements due to clouds or low thermal contrast. For example, Fig. 1b has one missing day (N=23 satellite measurements) but with an otherwise even distribution throughout the remainder of the period, while Fig. 1c (N=24) has nearly the same number of satellite measurements as Fig. 1b but clustered on only 8 of the 15 days.

290   Finally, there are also many cases where selected day(s) have few or no IASI measurements at all (Fig. 1d). When neither temporal coverage nor the number of IASI pixels are high, one can still calculate the matched IASI NH_3 column for this AMoN sample, but the result is unlikely to be more as representative than as a more temporally distributed comparison.

295
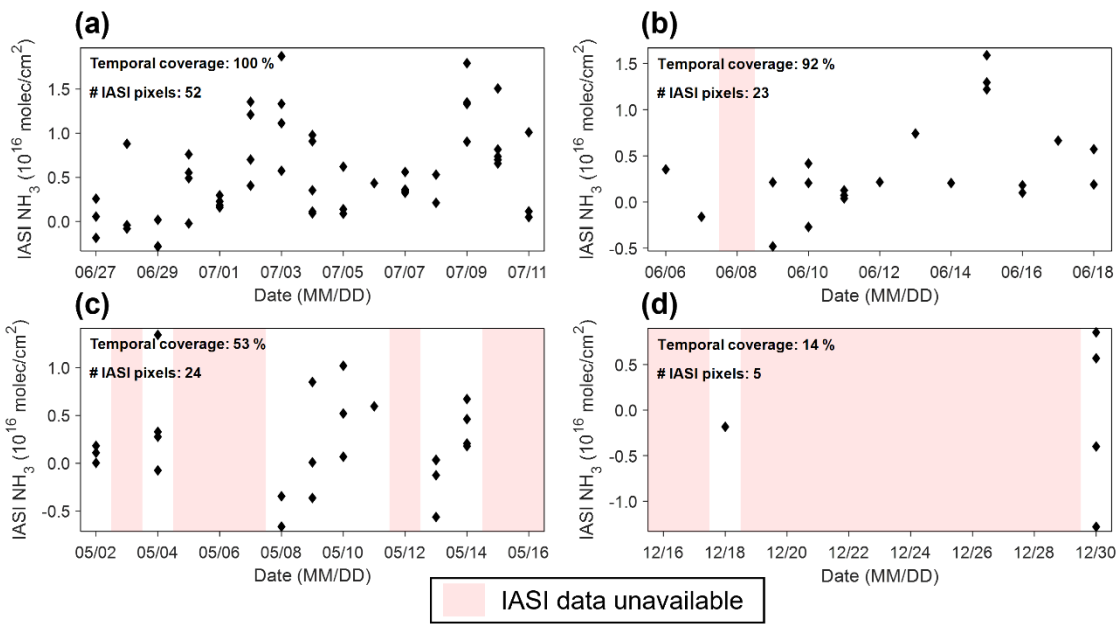
Figure 1. Examples of IASI data temporal coverage over the biweekly AMoN sampling period for an AMoN site in Yosemite National Park, California (CA 44): **(a)** several IASI measurements every day during the 2-week sampling period; **(b)** a few IASI measurements for most time days of the 2-week sampling period; **(c)** many IASI measurements but only in several days during the 2-week sampling period; **(d)** sparse IASI measurements for only several days during the 2-week sampling period.

300

To this end, we explore the dependence of the correlation between IASI and AMoN with on IASI data's temporal coverage of the 2-week sampling period and total number of IASI pixels within the 2-week AMoN sampling period, using the 25 km spatial window. For example, the temporal coverages for Fig. 1 are 100%, 92%, 53%, and 14%, respectively, and the number of IASI pixels are 52, 23, 24, and 5, respectively. The impact of different temporal averaging and the number of IASI pixels

requirements are summarized in Table 2 and Table 3, respectively. Increasing temporal coverage and number of IASI pixels both yield higher r values than any of the simple spatial windows alone. Table 2 shows that the correlation improves to r = 0.74 when the temporal coverage is ≥ 80%, suggesting a significant impact of temporal coverage of the IASI data. The IASI and AMoN correlations also increase over a simple spatial window with increasing numbers of IASI pixels, yet the impact is not as strong (r = 0.63 for N ≥ 40) as the sensitivity to temporal coverage.

Table 2. The impact of IASI data's temporal coverage for the 2-week AMoN sampling period (25 km spatial window)

IASI temporal coverage per AMoN-IASI pair (%)	[0, 20)	[20, 50)	[50, 80)	[80, ∞)
r	0.17	0.29	0.47	0.74
Mean # IASI pixels per AMoN-IASI pair	3	13	26	38
# AMoN-&-IASI pairs	1766	7641	5137	999

Table 3. The impact of # IASI pixels (25 km spatial window)

# IASI pixels per AMoN-IASI pair	[0, 10)	[10, 20)	[20, 40)	[40, ∞)
r	0.16	0.37	0.50	0.63
Mean temporal coverage per AMoN-IASI pair (%)	22	42	61	80
# AMoN-&-IASI pairs	4533	5025	5309	676

Because the temporal coverage and number of IASI pixels are not independent variables, additional analyses are conducted to study the sensitivity of these two effects using Monte-Carol method. First, the available dataset is filtered to cases when at least one of the fourteen days have multiple IASI measurements per AMoN measurement, at least 7 days of the 14-day sampling period had at least one IASI measurement, and the total number of IASI pixels is at least 20. The number of days with available IASI measurement is denoted by T. Two opposite approaches are explored for 104 qualified AMoN sites:

325 (1) Maximized temporal coverage (TC_max): only one IASI pixel is randomly selected to represent that day, and the total number of IASI pixels equals T (T≤14). In this case, the temporal coverage is maximized.

(2) Minimized temporal coverage (TC_min): only days with the largest number of IASI pixels are selected until the total number of IASI pixels equals T (T≤14). In this case, the temporal coverage is minimized, and the total number of selected
330 IASI pixels is same with TC_max.

For each AMoN site, we ~~performed~~ repeated the two different sampling strategies ~~for~~ 100 times, then calculated the median r value to represent each site using the maximum and minimum coverage approaches. Fig. 2a shows the histogram and normalized fit of change in r (Δr = TC_max-TC_min) for each site between the two scenarios with the number of bins
335 determined by Sturge's rule. The increased correlation of Δr = 0.45 ± 0.28 shows the large impact of temporal coverage. The total number of IASI pixels used for the two strategies were identical.

To further investigate the impact of including more IASI pixels after maximizing temporal coverage, we also test the process described in (1) and then randomly added (20-T) more IASI pixels from the remaining IASI pixels and referred to it as
340 TC_max_add. Fig. 2b shows that the changes Δr between TC_max and TC_max_add are small (-0.00 ± 0.05). For the TC_max strategy, the initial number of IASI pixels was between 7 and 14, which means using TC_max_add strategy result in a 43 ~ 186 % increase in the number of IASI pixels compared to TC_max alone. Adding more IASI pixels does not have a significant impact on the r values, indicating that maximized temporal coverage alone is the most important factor when comparing IASI to AMoN stations.
345

After applying a temporal coverage requirement (temporal coverage ≥ 80 %) to filter the overall dataset, we revisit the sensitivity of the agreement between spatial windows. The smaller spatial window now yields better agreement than the larger spatial windows (Table 4). Compared with Table 1 which has no filter for temporal coverage, the r values in Table 4 increase for all spatial windows. The correlations are clearly better for smaller spatial windows (r = 0.74 for 25 km versus r = 0.48 for
350 100 km). In this way, the use of a larger spatial window is indeed a tradeoff between the increasing temporal coverage versus incorporating a larger spatial gradient. The results further demonstrate that the IASI pixels far from the AMoN sites may not be representative to the AMoN site.

355
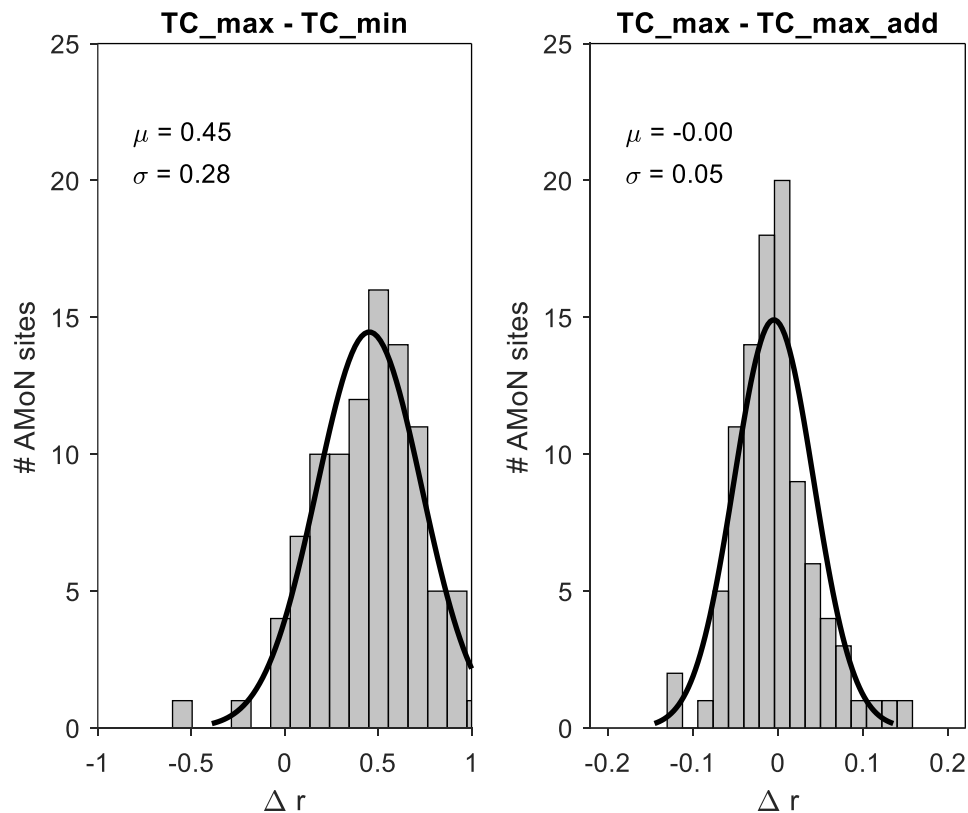
Figure 2. The change in r values for individual AMoN sites using different sampling strategies: **(a)** maximized temporal coverage (TC_max); minimized temporal coverage (TC_min) and **(b)** maximized temporal coverage & randomly adding more pixels (TC_max_add).

360

Table 4. AMoN & IASI comparison results for different spatial windows (temporal coverage ≥ 80 %)

Spatial window	15 km	25 km	50 km	100 km
Pearson's r	0.76	0.74	0.58	0.48
Mean # IASI pixels per AMoN-IASI pair	19	38	119	392
# AMoN- & IASI pairs	105	999	3138	6899

3.3 Sensitivity to seasons and temporal averaging

365 AMoN has similar numbers of measurements in spring (March, April, May), summer (June, July, August), autumn (September, October, November), and winter (December, January, February), while the mean number of IASI pixels (# IASI pixels) per pair in winter is only around half of other seasons (Fig. 3). In winter, low thermal contrasts result in low sensitivity of thermal infrared sounder, which explains the low number of IASI pixels in winter (Clarisse et al., 2010; Guo et al., 2021). The lower sensitivity of the infrared thermal sounder measurements in winter results in higher uncertainties, and thus comparisons

370 between IASI and AMoN are especially important. When temporal coverage is at least 80%, IASI wintertime data still have good agreement with AMoN (r = 0.61) although the comparison ~~are~~is limited to only a few AMoN & IASI pairs (N = 33). The r values for spring, summer, and autumn when temporal coverage $\geq$ 80% are 0.60 (N = 181), 0.76 (N = 502), and 0.70 (N = 283), respectively. IASI in general only provides a small number of pixels in winter, however, it indeed has the capability of reflecting surface NH_3 variations even in winter.

375
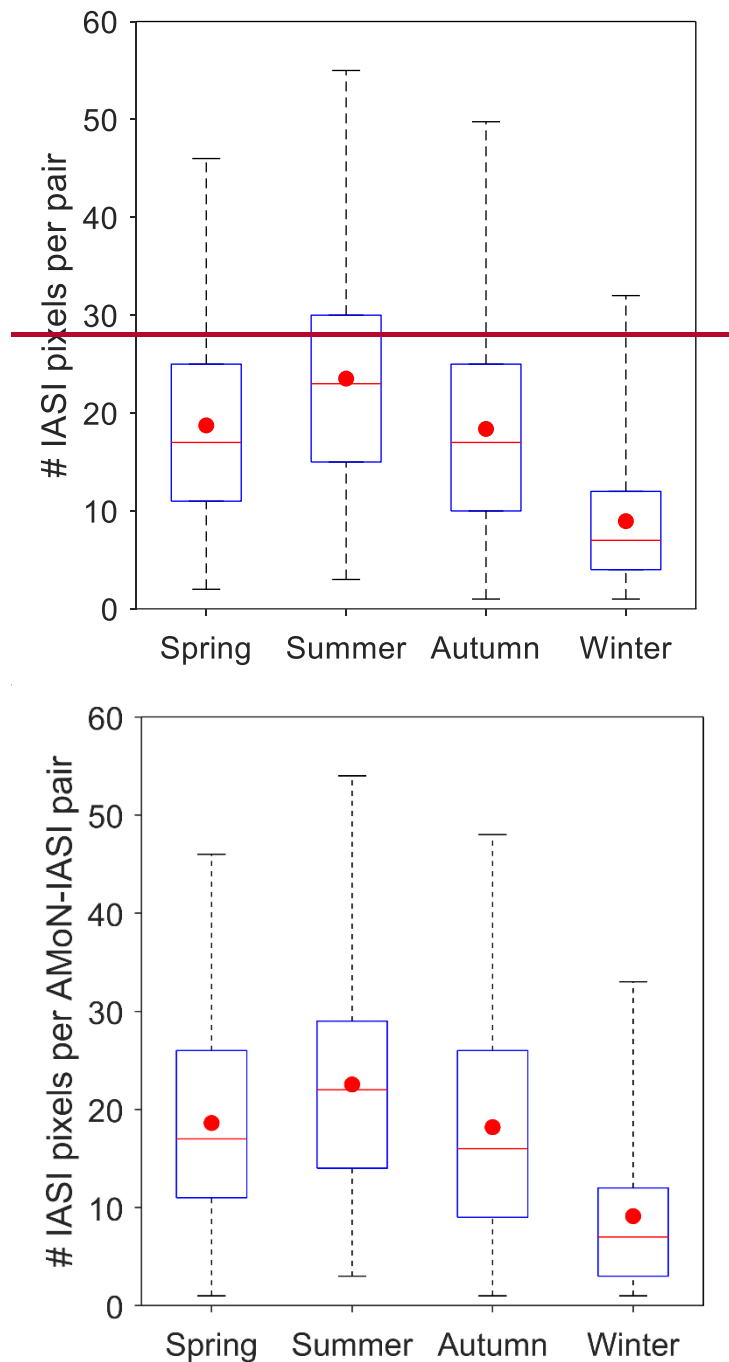
Figure 3. Boxplot of number of IASI pixels per AMoN-IASI pair for spring, summer, autumn, and winter. The boxes denote the 25th and 75th percentiles, the whiskers denote the 1st and 99th percentiles, and the red dot denotes the mean.

380

The results in 3.1 and 3.2 have already shown the importance of spatial window and temporal coverage. The temporal averaging and regridding approaches, such as the tessellation oversampling and physical oversampling, ~~is~~ are ~~a~~ common method~~s~~ to achieve ~~a~~ higher spatial resolution ~~map~~ by sacrificing the temporal resolution (Sun et al., 2018; Van Damme et al., 2018; Wang et al., 2021). Here we neglect the interannual variability of NH$_3$ seasonality and calculate ~~the multi-year~~ averaged

385   IASI and AMoN NH$_3$ seasonality during 2008 - 2018~~concentrations~~ using the 25 km spatial window. By averaging the multi-year IASI data, the impacts of temporal coverage are alleviated because both temporal coverage~~s~~ and numbers of IASI pixels increase. Among the 101 AMoN sites with at least one full year data and available IASI v3.1r NH$_3$ data, 49 sites show strong agreement with IASI with r > 0.8, 29 sites have moderate agreement of 0.5 < r ≤ 0.8, while 23 sites do not have statistically significant agreements (Fig. 4a). If taking all data into consideration, the overall r value for the CONUS is 0.69. The AMoN

390   sites with higher NH$_3$ concentrations tend to show better agreements between AMoN and IASI (Fig. 4b). The median AMoN NH$_3$ annual mean concentrations for all sites is 0.86 μg/m^3. Most sites with no statistically significant agreements have a low NH$_3$ concentration (median: 0.48 μg/m^3). Currently, most AMoN sites are located in low or moderate NH$_3$ concentration regions with a lack of sites in the NH$_3$ hotspots (Wang et al., 2021) and urban areas, complicating the comparison between AMoN and IASI.

395

The above agreement demonstrates that IASI NH$_3$ column reflects the variation of the surface NH$_3$ concentration at seasonal resolution. For regions without any available ground measurements, IASI NH$_3$ observations can be used to help better understand the NH$_3$ variations. However, large differences exist among the relationships between IASI and AMoN NH$_3$ concentrations over different AMoN sites (an example of linear regression plot in Fig. 5b). Even for AMoN sites with excellent

400   correlation (r > 0.8), the slopes vary a lot, ranging from 0.08 – 1.4 × 10^{16} molec/cm^2 per μg/m^3. For instance, two AMoN sites in California, Joshua Tree National Park (CA 67) and Sequoia & Kings Canyon National Park (CA 83), both exhibit great seasonality agreements with IASI (r = 0.97 and r = 0.99, respectively) but the slope for CA 83 (Fig. 4d) is 44 % higher than CA 67 (Fig. 4c). The difference between the slopes suggests that although IASI is able to capture the general seasonality, the relationship between NH$_3$ column and surface NH$_3$ is distinctly different due to complicated topography, meteorology, and

405   other factors at different AMoN sites.
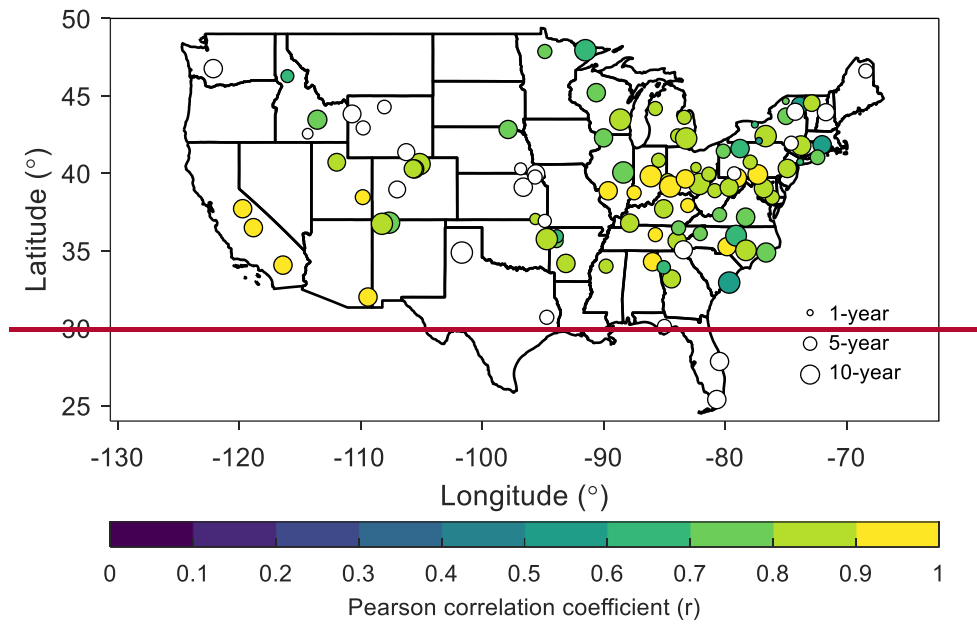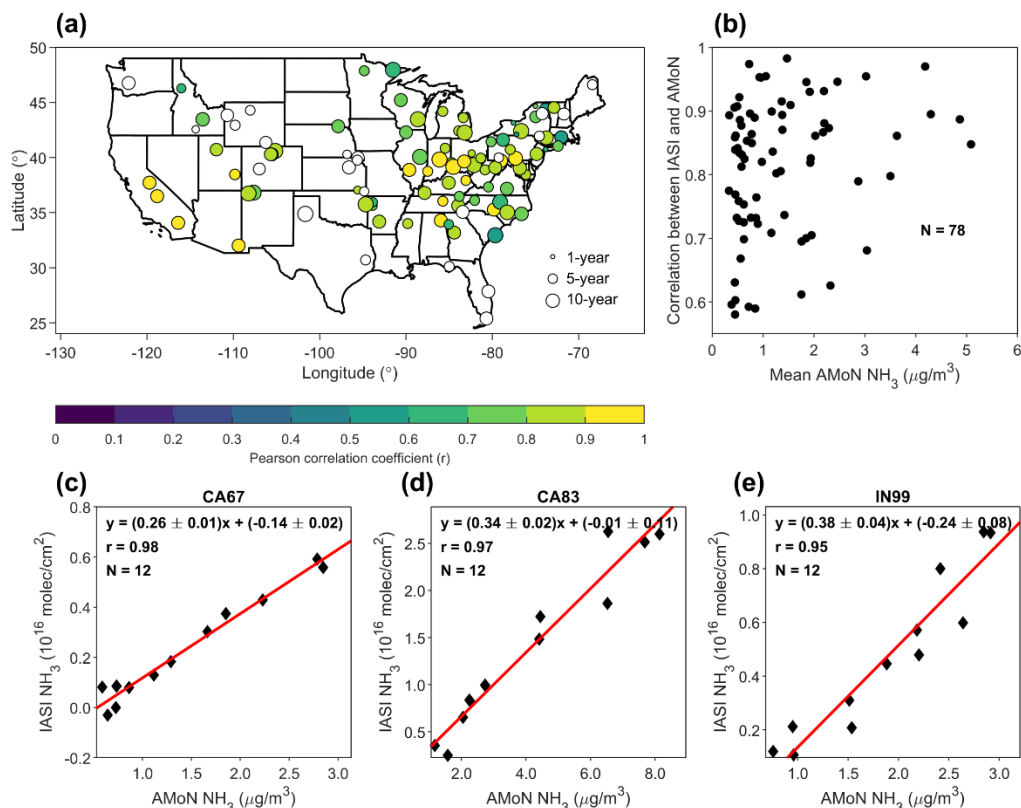
Figure 4. (a) Multi-year averaged NH₃ seasonality comparison results between AMoN sites and the IASI observations within 25 km of the AMoN sites at monthly resolution. Circles without filled color denote the AMoN sites with no statistically significant correlation with IASI (α = 0.05). The circle sizes denote the length of AMoN data record~~;~~. (b) The relationship between mean AMoN NH₃ concentrations and the correlation between AMoN and IASI seasonality; The regression between IASI and AMoN observed NH₃ seasonality for (c) the AMoN site in Joshua Tree National Park, California (CA67), (d) the AMoN site in Sequoia National Park, California, and (e) the AMoN site in Indianapolis, Indiana (IN99).

4 Trend analysis

4.1 Trend in the CONUS

Strong evidence of increasing NH₃ concentrations in the U.S. comes from both ground-based observations and satellite measurements (Van Damme et al., 2021; Warner et al., 2017; Yao and Zhang, 2016; Yao and Zhang, 2019; Yu et al., 2018). The methodology and comparison results in section 3 demonstrate that IASI NH₃ can be used to ~~estimate~~ verify and augment regional NH₃ trends over the last decade. ~~In this regard,~~Here we will compare satellite ~~IASI NH₃ observations~~ trends with~~will be used to augment the AMoN observed NH₃ trends in the CONUS over the last decade. We include AMoN trend analysis~~

 Fig. 5~~a~~ shows monthly averaged IASI and AMoN timeseries ~~in~~ from Indianapolis, Indiana, USA (IN 99). The strong correlation (r = 0.96) between the two measurements is shown in Fig. 5b. Although the NH₃ seasonality remain consistent from 2008 to 2018 - namely spring maxima and secondary maxima in fall with lowest values in winter - both AMoN and IASI also show increasing trends of NH₃ concentrations over the entire timeseries. AMoN shows a trend of $6.5\%\cdot yr^{-1}$ while IASI shows a trend of $7.0\%\cdot yr^{-1}$.
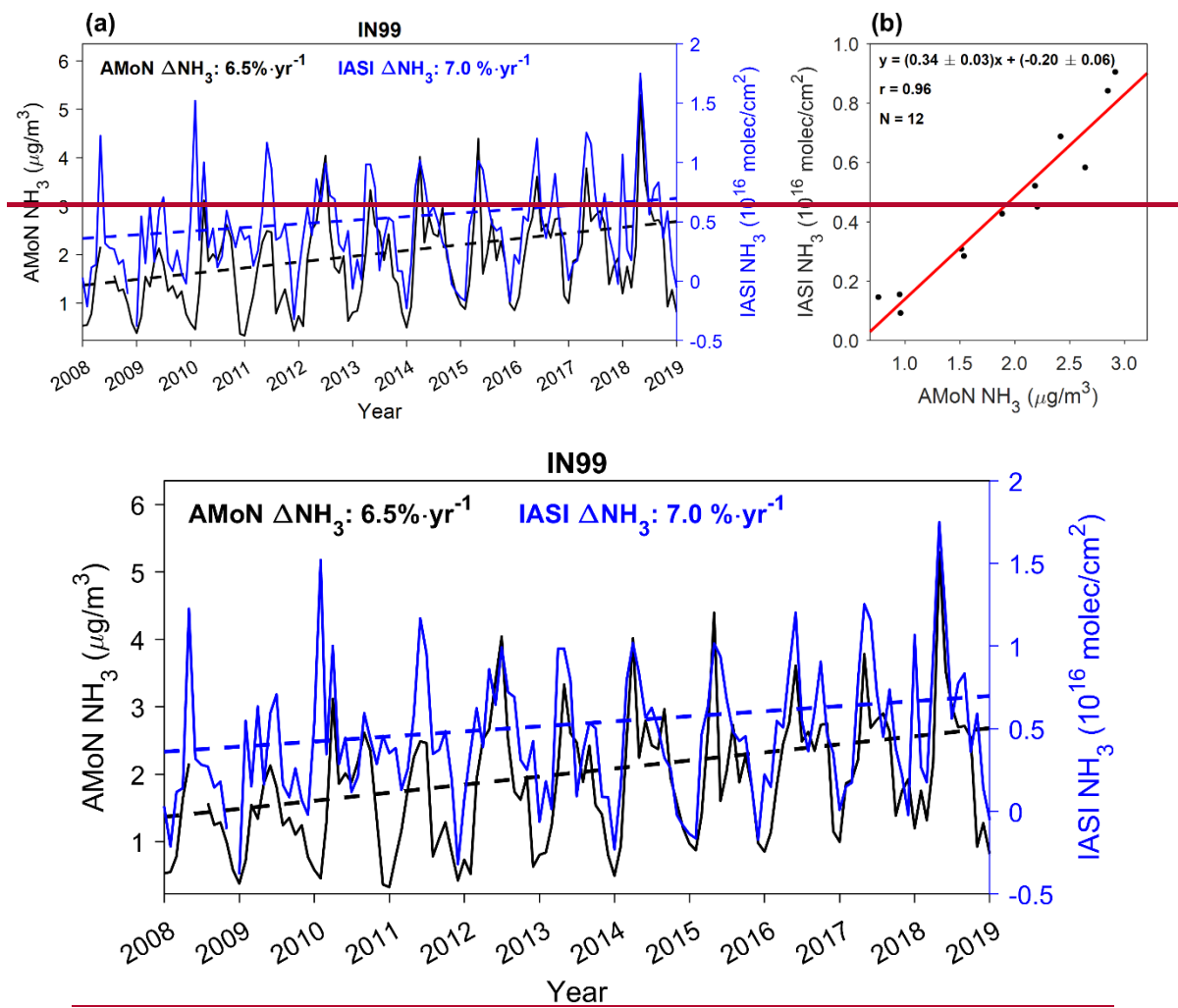
Figure 5. ~~(a)~~ 2008 – 2018 trends in monthly averaged NH₃ ~~trends~~ for AMoN site in Indianapolis, Indiana, U.S. (IN 99) and IASI NH₃ observations within 25 km of IN 99~~; (b) seasonality correlation between AMoN and IASI NH₃ for IN 99.~~

435 Here we will compare IASI NH₃ trends with the AMoN observed NH₃ trends in the CONUS over the last decade. We include AMoN trend analysis only for sites with full year coverage during 2008 - 2018 (N=13). To achieve a higher spatial resolution, in the following study, we used the oversampled IASI NH₃ maps to calculate NH₃ trend for each 2 km grid box. A long-term trend analysis was then performed using AMoN and IASI oversampled data (Sun et al., 2018; Wang et al., 2021) by Theil-Sen's slope estimator and MK test to examine the agreement between the datasets and explore any regional differences. IASI

440 NH₃ columns smaller than the 5th percentile (0.5×10^{15} molec/cm^2) of the 11-year NH₃ average in the CONUS region were excluded to avoid spurious trend results caused by the higher noise in these measurements. To perform the interannual trend analysis, we require each region or site to have at least one valid measurement in each season to alleviate the possible bias due to seasonal variations. Fig. 6 shows the annual percentage change for both IASI and AMoN. Most regions in the CONUS have increasing NH₃ concentrations based on the 11-year IASI observations (median: 6.8% · yr^{-1}), including eastern U.S., Midwest,

445 and parts of the western U.S. 10 out of 13 AMoN sites have statistically significant NH₃ increases. AMoN data in general suggest similar increases (median: 6.7% · yr^{-1}). When plotting the trends of AMoN sites against the median of IASI trends within a 25 km spatial window (Fig. 7), a moderate correlation (r = 0.66) was found between IASI and AMoN NH₃ trends. IASI in general suggested a higher NH₃ increase compared to AMoN (slope: 1.26 ± 0.51) with the ratio larger than one for most sites. ~~The absolute NH₃ change also is in correspondence with the previous study, with significant NH₃ increases across~~

450 ~~the CONUS regions, especially in the Midwest (Van Damme et al., 2021).~~

The spatial consistency across the datasets differs significantly. Both AMoN and IASI suggest ~ 5% · yr^{-1} NH₃ increases in the Great Lake Region, while IASI suggests a higher NH₃ increase in the eastern US compared with AMoN. The IASI trend analysis results suggest a significant NH₃ increase in the northern Great Plains, e.g., North Dakota, South Dakota, and Montana,

455 yet there are no AMoN sites in this region. Furthermore, the trends are consistent with the NH₃ emissions increases caused by increased N fertilizer usage in the northern Great Plains (Cao et al., 2020b). McHale et al. (2021) showed that wet-precipitation NH₄$^+$ concentrations based on NADP observations suggested the highest increases in the Great Plains, the Rocky Mountain Region, and the Great Lake Region from 2000 to 2017, which is geographically consistent with the NH₃ trends observed by both AMoN and IASI. Here we note that the spatial resolution could affect the results of trend analyses. The trend 6.8% · yr^{-1}

460 was derived as the median of trends for each 2 km grid box. If considering the CONUS as a whole and calculating the annual mean NH₃ for the whole CONUS during 2008 – 2018 to derive the overall trend in CONUS, the IASI NH₃ change for 2008 – 2018 is (3.9 ± 2.2) % · yr^{-1} and $(1.3 \pm 0.8) \times 10^{14}$ molec/cm^2·yr^{-1}, similar with the trend in the previous study (3.4 ± 0.6) % · yr^{-1} and $(1.1 \pm 0.4) \times 10^{14}$ molec/cm^2·yr^{-1}) (Van Damme et al., 2021).

465

We use Hoshen–Kopelman algorithm to cluster adjacent grid points above the 95th percentile threshold of the 11-year CONUS oversampling map (6.7×10^{15} molec/cm^2) as a NH₃ hotspot (Hoshen & Kopelman, 1976; Wang et al., 2021), and the median area of identified hotspots is ~ 150 km^2 (Wang et al., 2021). ~~In terms~~Analyzing ~~of trend in~~ NH₃ hotpots, ~~which are here defined~~

as ~~regions where the IASI NH₃ column is larger than the 95ᵗʰ percentile of 11-year CONUS map (6.7 × 10¹⁵ molec/cm²),~~ the
median of NH₃ trend is 4.7% · yr⁻¹, indicating that the regions of the largest emissions sources are also ~~realizing~~ seeing
increasing concentrations over time. Although the percent changes in the regions with the highest concentrations are smaller
~~compared with~~than the trend in the CONUS median (~~8.0~~6.8% · yr⁻¹), in terms of the absolute changes, the median trend of
NH₃ columns over these NH₃ hotspots are higher ~~compared with~~than the trend in the CONUS median (3.7×10^{14} molec/cm²·yr⁻¹ vs. 2.8×10^{14} molec/cm²·yr⁻¹). The top 10 NH₃ hotspots in CONUS regarding column-areal weighting (NH₃ column times
the area) all exhibit increasing NH₃ concentrations from 2008 to 2018 (Table 5). Within these hotspots, the central Great Plains
experience the largest NH₃ increase (median: 5.0% · yr⁻¹, 4.0×10^{14} molec/cm²·yr⁻¹) while the San Joaquin Valley (median:
2.0% · yr⁻¹, 1.6×10^{14} molec/cm²·yr⁻¹) and Imperial County, California (median: 2.1% · yr⁻¹, 1.9×10^{14} molec/cm²·yr⁻¹) ~~have~~
see the~~a~~ ~~smaller~~smallest change~~s~~.

480
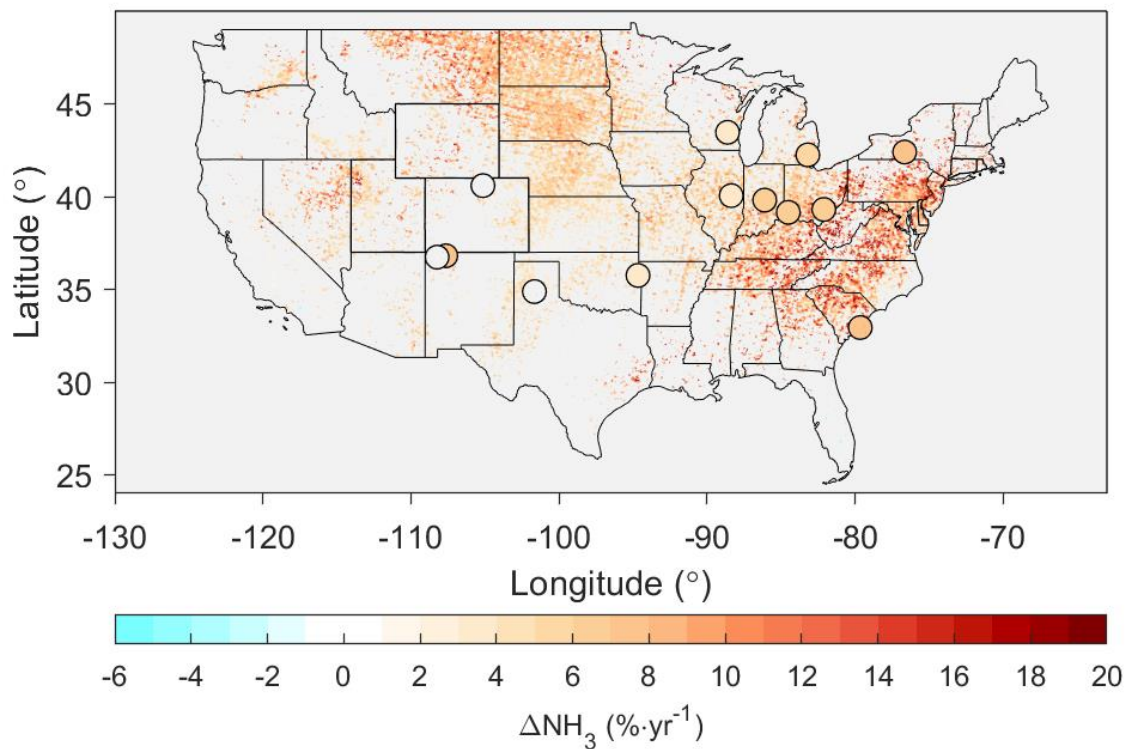
Figure 6. Trend analysis for IASI NH₃ (2008 - 2018) and AMoN NH₃ measurements in the contiguous U.S. The gray color indicates no
statistically significant change (α=0.05). ~~The circle size denotes the length of AMoN data record.~~

Figure 7. Comparison between 2008 - 2018 AMoN and IASI NH$_3$ trends (25 km spatial window) for AMoN sites with available nearby IASI trend data
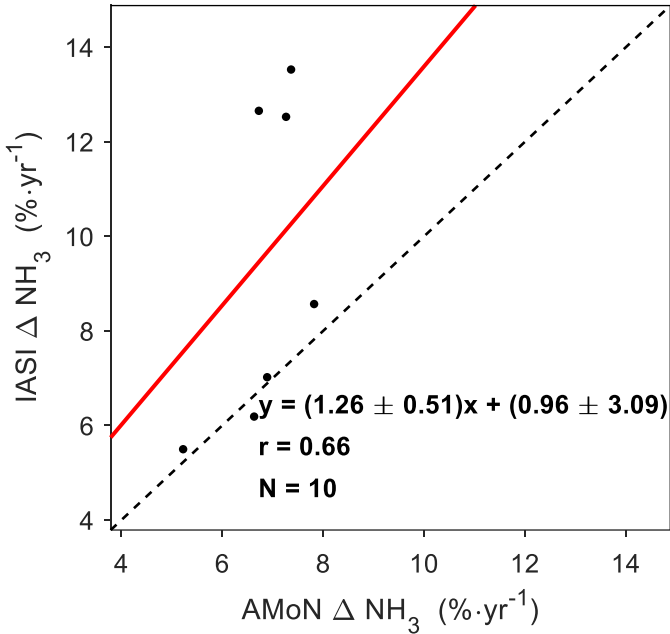
Table 5. 2008 – 2018 IASI observed NH$_3$ trend in the top 10 NH$_3$ hotspots (column-areal weighting) in CONUS

Hotspots	$\% \cdot yr^{-1}$	10^{14} molec/cm$^2 \cdot yr^{-1}$
Central Great Plains	5.0	4.0
The San Joaquin Valley	2.0	1.6
North Oklahoma	3.9	2.9
Texas panhandle	3.6	2.8
Central Iowa	4.4	3.3
The Snake River Valley	3.8	3.3
Southeast Iowa	5.2	3.9

Beadle County, South Dakota	8.3	6.0
Weld County, Colorado	3.6	2.9
Imperial County, California	2.1	1.9

490

To provide a detailed insight of the increasing NH_3 over the CONUS, we further perform trend analyses for different seasons (Fig. 8). In spring, significant NH_3 increases are found in the Midwest and ~~in the E~~e~~e~~astern US. In summer, NH_3 increases shift to the western US and ~~part of the~~the eastern ~~Northeast~~ US. AMoN and IASI seasonality clustering results show that the Midwest and eastern United States, dominated by fertilizer NH_3 emissions, have a broad, spring maximum of NH_3, while the

495 western United States, dominated by volatilization of livestock waste NH_3 emissions, in contrast, show a narrower midsummer peak (Wang et al., 2021). The spatial patterns of spring and summer NH_3 trends are in agreement with the seasonality clustering results, indicating that increasing NH_3 emissions caused by agricultural activities may contribute to NH_3 concentration increase. The increasing wildfire activities in the western U.S. may also contribute to NH_3 increases (Lindaas et al., 2021a, b). In fall and winter, most regions in the U.S. do not have statistically significant IASI NH_3 trends, and a decreasing NH_3 trend

500 is observed by IASI in the Southwest US in fall. In contrast, AMoN data suggest a notable NH_3 increase in Northeast and the Corn Belt region in winter. Again, IASI data are susceptible to low thermal contrasts in winter, which to some extent explains the disagreement between IASI and AMoN in winter as discussed in Section 3.3.

Wintertime NH_3 plays an important role in haze episodes through the formation of aerosol phase NH_4NO_3 (Shah et al., 2018;

505 Zhai et al., 2021), and increasing NH_3 concentrations in winter may affect aerosol acidity and aerosol chemistry (Lawal et al., 2018; Zheng et al., 2020). In the past decades, NO_x and SO_2 emissions reductions have resulted in less NH_x partitioning into particle phase NH_4^+ (Shah et al., 2018), however, the partitioning alone is not able to fully explain the significant NH_3 concentration increases (Yao and Zhang, 2019; Yu et al., 2018). The change of meteorological conditions, such as increasing air temperatures may also contribute to the increasing NH_3 trends (Warner et al., 2017; Yao and Zhang, 2019). No matter the

510 reason for increasing NH_3 concentrations across the CONUS regions, the fact that both NH_3 surface concentrations and NH_3 column concentrations are increasing during the past decade will have significant impacts on air quality and nitrogen deposition. EPA is reviewing the 2020 $PM_{2.5}$ National Ambient Air Quality Standard (NAAQS) currently set at 12.0 $\mu g \cdot m^{-3}$ and if the NAAQS is lowered, NH_3 controls will become increasingly important for meeting the standard. Additionally, Pan et al. (2021) demonstrates that NH_3 transported from Colorado significantly increased the dry NH_3 deposition the Rocky

515 Mountain National Park. Increasing gas phase NH_3 may result in longer spatiotemporal scales for dry nitrogen deposition, leading to adverse impacts on remote regions and sensitive ecosystems (Phoenix, et al., 2006). Reduction of NH_3 emissions is critical to protect human health and the biodiversity in sensitive ecosystems (Ellis et al., 2013, Hill et al., 2019).
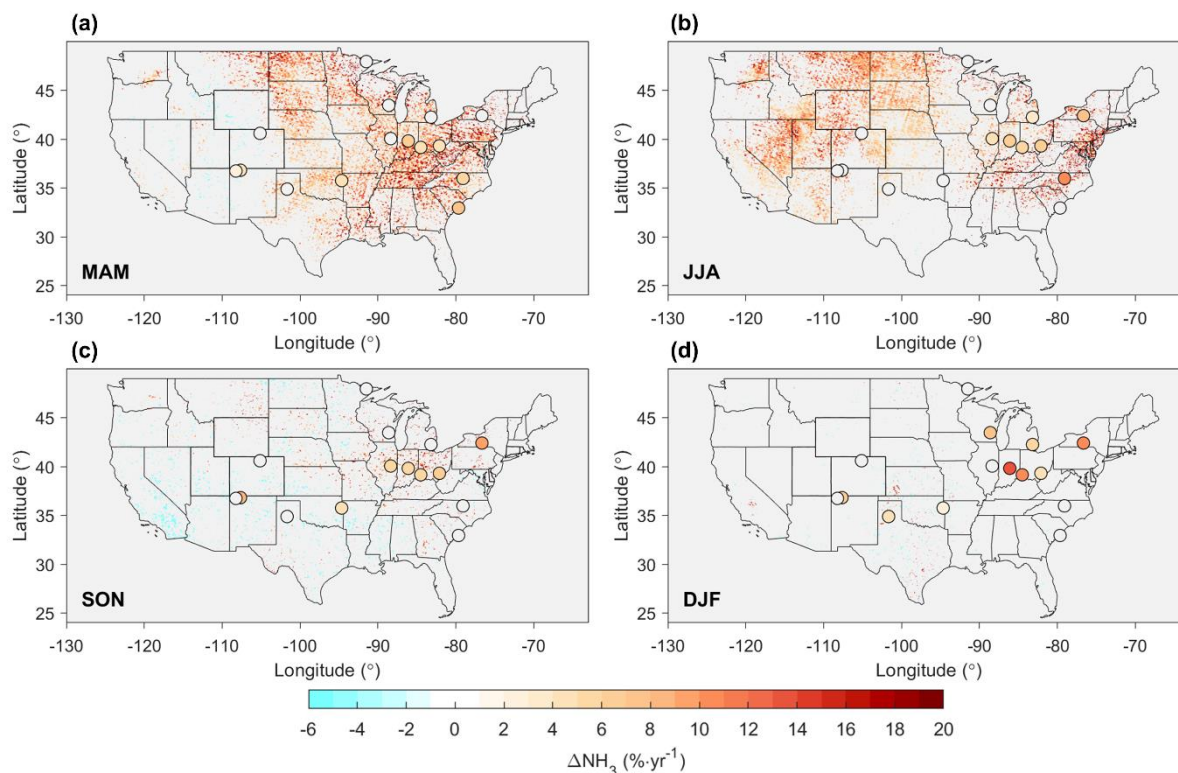
Figure 8. 2008 – 2018 NH₃ trend for different seasons based on IASI NH₃ measurements in the contiguous U.S. **(a)** spring (March, April, May); **(b)** summer (June, July, August); **(c)** autumn (September, October, November); **(d)** winter (December, January, February). The gray color indicates no statistically significant change (α = 0.05).

4.2 Trend in the urbanized areas

The short lifetime of NH₃ leads to strong spatial variabilities of NH₃ concentrations, and most AMoN sites are not located in highly populated urban regions (Wang et al., 2021), a gap that IASI data can fill. Fig. 9a shows the cumulative distribution of the US population as a function of the distance from an AMoN site~~population coverage of AMoN in the CONUS region~~. Population data were retrieved from the Gridded Population of the World, Version 4 (GPWv4) (Center for International Earth Science Information Network – Columbia University, 2018). More than half of the CONUS population is at least 100 km away from an AMoN site. As mentioned in the previous discussion of spatial windows, AMoN may best represent the NH₃ variations for regions within ~ 10 km radius, and less than 2% of CONUS population are within 10 km of an AMoN site. More urban AMoN sites are needed to represent the urban areas and better quantify NH₃ emissions from mobile sources and~~,~~ trends ~~in~~ in population centers~~the urban areas~~. Satellite observations are the only dataset that can currently be used to investigate source contributions and trends in population centers (Cao et al., 2022).

535 We retrieved urban area data from the 2010 US Census, which includes two different types of urban areas: Urbanized Areas (UAs) of 50,000 or more people and Urban Clusters (UCs) of at least 2,500 and less than 50,000 people (U.S. Census Bureau, 2012). The urban areas have a similar NH_3 trend compared with CONUS (8.1% · yr^{-1} vs. ~~8.0~~6.8% · yr^{-1}), suggesting a simultaneous NH_3 increase in both urban and rural areas. The top ten most populous urbanized areas almost all exhibit significant NH_3 increases with the exception of Miami, Florida, which has a negative trend and Dallas, Texas, without any

540 significant trend (Table 6). These ten areas in total ~~accommodate~~ account for more than seventy million people~~population~~, making up more than one fifth of the total population in the CONUS. The urban environment with abundant HNO_3 and NH_3 emissions from vehicles favors the formation of NH_4NO_3. Recent studies suggest that gas phase NH_3 hinders the scavenging of NH_4NO_3 by slowing down the deposition process of total inorganic nitrate (Zhai et al., 2021) and promotes new atmospheric particle formation by directly nucleate with HNO_3 to form NH_4NO_3 in winter in urban areas and (Wang et al., 2020). However,

545 ultimately the sensitivity to $PM_{2.5}$ from increases in NH_3 in any urban areas will be a complex function of trends of NO_x and SO_2 as well (Feng et al., 2020). The NH_3 increase in these densely populated areas and its impact on ~~the~~ aerosol chemistry ~~need~~needs to be further addressed. For example, Fig. 9b shows the relationship between NH_3 trends versus emissions trends (EPA Air Pollutant Emissions Trends Data) on the state level. For agricultural areas with high NH_3 (excess NH_3 relative to NH_4NO_3 equilibrium), one would expect an increase in emissions to correlate very well with increasing NH_3 columns. In

550 contrast, in areas with more NO_x, increases in emissions may result in NH_3 going into NH_4NO_3 and thereby show little or even negative correlations. To this end, Fig. 9b shows that at state level, states with strong agricultural emissions show strong correlations between emissions and concentrations trends, e.g., Iowa, while northeast states show weak or negative correlations, e.g., New Jersey. Ultimately, co-located aerosol phase and gas phase precursor measurements are needed to fully deduce what is happening at each urban area and should be a focus of future air quality network integration.

555
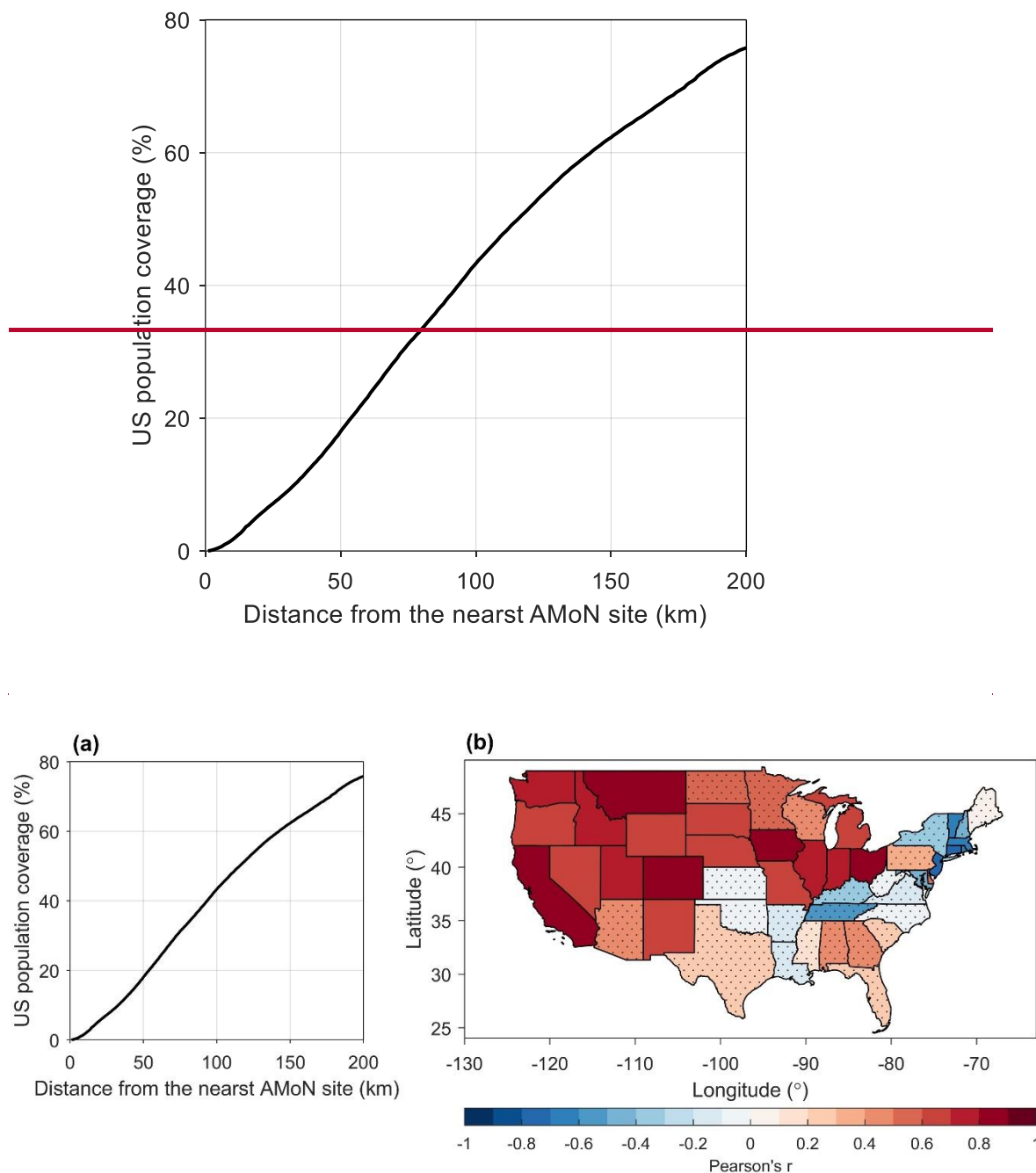
Figure 9. (a) Cumulative distribution of CONUS population as a function of distance from~~The population coverage of~~ the nearest AMoN sites~~s~~; (b) Correlation between EPA NH$_3$ emissions and IASI observed mean NH$_3$ concentrations at state level during 2008 - 2018. The gray dots represent states without statistically significant correlations ($\alpha = 0.05$).

Table 6. 2008 – 2018 IASI NH$_3$ trend in the top 10 most populous urbanized areas

Urbanized Area	Population (million)	% · yr^{-1}	10^{14} molec/cm^2 · yr^{-1}
New York--Newark, NY--NJ--CT	18.0	10.8	2.0
Los Angeles--Long Beach--Anaheim, CA	12.0	4.3	2.1
Chicago, IL--IN	8.6	5.2	2.5
Miami, FL	5.5	-25.2	-1.5
Philadelphia, PA--NJ--DE--MD	5.4	10.9	2.6
Dallas--Fort Worth--Arlington, TX	5.1	/	/
Houston, TX	4.9	7.9	2.0
Washington, DC--VA--MD	4.6	9.0	2.2
Atlanta, GA	4.5	9.4	2.2
Boston, MA--NH--RI	4.2	10.5	1.4

5 Implications

Under favorable conditions, IASI NH$_3$ columns correlate with AMoN NH$_3$ surface concentrations even at the 2-week scale
and for low concentration regions (r = 0.74 when temporal coverage ≥ 80 %). The temporal coverage of IASI measurements'
data during the 2-week temporal coverage of AMoN's 2 week sampling period is the controlling factor of the correlation
between IASI and AMoN measurements, dominates the agreement presumably because of the larger day-to-day variability of
NH$_3$. The agreement demonstrates the strong potential for using IASI NH$_3$ columns to bridge the spatial gaps of the AMoN

network. The global coverage of satellite measurements enables the IASI NH$_3$ product to serve as an alternative dataset in countries and regions that do not have any NH$_3$ monitoring networks, particularly in developing countries. For example, India is the second most populated country in the world with a sixth of the world's population, and recent study has shown that the unique role of NH$_3$ in forming massive chloride aerosols (up to 40 μg/m^3) in India (Gunthe et al., 2021). However, there are currently no long-term NH$_3$ ground monitoring networks in India, impeding the efforts to estimate and control NH$_3$ emissions (Beale et al., 2022). IASI's low sensitivity to wintertime NH$_3$ shows the value of the more sensitive AMoN sites. Extra attention is needed when using IASI data in such circumstances.

The increasing NH$_3$ in the CONUS (median: 6.8%·yr^{-1}, 2.8×10^{14} molec/cm^2·yr^{-1}), including the hotspots region (median: 4.7%·yr^{-1}, 3.7×10^{14} molec/cm^2·yr^{-1}), highlights the more important role of NH$_3$ in PM$_{2.5}$ formation and nitrogen deposition in the future. AMoN suggests a similar NH$_3$ increase (6.7%·yr^{-1}) as well as a similar spatial patterns with IASI. Both IASI and AMoN show largest NH$_3$ increases in the Midwest and eastern U.S., with a moderate agreement correlation between the IASI and AMoN trends for the entire CONUSAMoN sites (r = 0.66). More co-located measurements of PM$_{2.5}$ mass and NH$_3$ concentrations would help assess the impact increasing trends of NH$_3$ will have on human health. The integrated satellite and ground-based measurements are already playing a role in our understanding of under-represented NH$_3$ emissions sources in the inventories. NH$_3$ already dominates the reactive nitrogen deposition in the majority areasmost regions in the U.S., with the continuing efforts on NO$_x$ emission reductions, NH$_3$ is expected to become the key species for nitrogen deposition (Li et al., 2016), which will have and poses adverse impacts on the nearby ecosystem regions, e.g., the National Parks (Benedict et al., 2013; Pan et al., 2021). The changing partitioning of NH$_x$ between NH$_3$ and NH$_4^+$ is likely to impact the lifetime of NH$_x$ due to differences between the removal velocity of gas phase NH$_3$ via dry deposition and particle phase NH$_4^+$ wet deposition. The trends vary in different seasons, with NH$_3$ increases mainly in spring in the Midwest and eastern U.S. (cropland dominated) whileand in summer in the western U.S. (feedlot dominated), suggesting the impacts from agricultural activities and the necessity of developing regionally-specific emission control strategies.

Because of the scarcity of the ground monitoring sites in the urban areas, satellite NH$_3$ measurements are extremely valuable forto characterizinge NH$_3$ magnitude, seasonality, and trend in densely populated areas. Satellite observations suggests NH$_3$ increases across the U.S. urban areas (median: 8.1%). New York—Newark, NY--NJ--CT alone has more than eighteen million population, experiencing an 10.8 % · yr^{-1} NH$_3$ increase. Measurements from satellites will help inform where ground based NH$_3$ samplers could be located to better understand local air quality in overburdened communities with limitedthat lack resources for continuous monitors. In addition, NH$_3$ sources in the urban areas and the related atmospheric chemistry are both poorly understood (Gu et al., 2022; Sun et al., 2017) and could be constrained by satellite NH$_3$ observations (Cao et al., 2022). However, satellite observations alone are not able to answer all questions under the complex urban atmospheric conditions. For instance, gas phase NH$_3$ and HNO$_3$ can nucleate directly to form NH$_4$NO$_3$ particles in cold atmospheric conditions and is likely to result in rapid growth of new atmospheric particles in winter in urban areas (Wang et al., 2020). The comparison

between NH$_3$ emission trends and IASI observed NH$_3$ concentration trends suggests that strong correlations exist in states with large NH$_3$ emissions from agricultural activities, e.g., Iowa, while weak or negative correlations in northeast states, e.g., New

610 Jersey, indicating the different contribution from emission and partitioning. To provide accurate and fine spatial scale NH$_3$ observations in the urban areas, more routine ground monitoring sites are needed both in urban areas and high NH$_3$ emission source regions.

6 Data availability

615 The AMoN data were downloaded from the National Atmospheric Deposition Program/National Trends Network (NADP/NTN): https://nadp.slh.wisc.edu/networks/ammonia-monitoring-network/. The authors acknowledge the AERIS data infrastructure (https://www.aeris-data.fr) for providing access to the IASI Level 2 NH$_3$ data used in this study. Population data were retrieved from Center for International Earth Science Information Network, Columbia University: https://sedac.ciesin.columbia.edu/data/collection/gpw-v4/. The urban areas data are downloaded from the U.S. Census Bureau:

620 https://www.census.gov/geographies/mapping-files.html. The emission trend data are downloaded form the US Environmental Protection Agency, Air Pollutant Emissions Trends Data: https://www.epa.gov/air-emissions-inventories/air-pollutant-emissions-trends-data.

Author contributions

MAZ and RW designed the research; RW led the analysis; KS, DP, and XG contributed to data analysis; LC, MV, LP, and

625 CC helped with the usage of IASI data; MP helped with the usage of AMoN data; and RW wrote the paper with contributions from all co-authors.

Competing interests

Competing interests. The contact author has declared that none of the authors has any competing interests.

Disclaimer

630 Publisher's note: Copernicus Publications remains neutral with regard to jurisdictional claims in published maps and institutional affiliations.

Acknowledgements

Xuehui Guo gratefully acknowledges the NASA Earth and Space Science Fellowship (Grant number: 80NSSC17K0377) for funding the work. We also gratefully acknowledge support for the analyses of the IASI and in situ data products from the

635 NASA Health and Air Quality Applied Sciences (HAQAST) team, NASA NNX16AQ90G. Mark A. Zondlo acknowledges support as a visiting scientist at ULB from the EUMETSAT Satellite Application Facility on Atmospheric Chemistry Monitoring (AC SAF). Kang Sun acknowledges the support from NASA Atmospheric Composition: Modeling and Analysis Program (ACMAP, Grant number: 80NSSC19K0988). The research was funded by the Belgian State Federal Office for Scientific, Technical and Cultural Affairs (Prodex HIRS) and the Air Liquide Foundation (TAPIR project). This work is also

640 partly supported by the FED-tWIN project ARENBERG ("Assessing the Reactive Nitrogen Budget and Emissions at Regional and Global Scales") funded via the Belgian Science Policy Office (BELSPO). L. Clarisse is Research Associate supported by the Belgian F.R.S.-FNRS. C. Clerbaux is grateful to CNES for scientific collaboration and financial support. The research presented was not performed or funded by EPA and was not subject to EPA's quality system requirements. The views expressed in this article are those of the author(s) and do not necessarily represent the views or the policies of the U.S.

645 Environmental Protection Agency.

References

Ahn, K. H. and Merwade, V.: Quantifying the relative impact of climate and human activities on streamflow, J. Hydrol., 515, 257–266, https://doi.org/10.1016/j.jhydrol.2014.04.062, 2014.

Beale, C. A., Paulot, F., Randles, C. A., Wang, R., Guo, X., Clarisse, L., Van Damme, M., Coheur, P.-F., Clerbaux, C.,

650 Shephard, M. W., Dammers, E., Cady-Pereira, K., and Zondlo, M.: Large sub-regional differences of ammonia seasonal patterns over India reveal inventory discrepancies, Environ. Res. Lett., https://doi.org/10.1088/1748-9326/AC881F, 2022.

Benedict, K. B., Day, D., Schwandner, F. M., Kreidenweis, S. M., Schichtel, B., Malm, W. C., and Collett, J. L.: Observations of atmospheric reactive nitrogen species in Rocky Mountain National Park and across northern Colorado, Atmos.

655 Environ., 64, 66–76, https://doi.org/10.1016/j.atmosenv.2012.08.066, 2013.

von Bobrutzki, K., Braban, C. F., Famulari, D., Jones, S. K., Blackall, T., Smith, T. E. L., Blom, M., Coe, H., Gallagher, M., Ghalaieny, M., McGillen, M. R., Percival, C. J., Whitehead, J. D., Ellis, R., Murphy, J., Mohacsi, A., Pogany, A., Junninen, H., Rantanen, S., Sutton, M. A., and Nemitz, E.: Field inter-comparison of eleven atmospheric ammonia measurement techniques, Atmos. Meas. Tech., https://doi.org/10.5194/amt-3-91-2010, 2010.

660 Bouwman, A. F., Lee, D. S., Asman, W. A. H., Dentener, F. J., van der Hoek, K. W., and Olivier, J. G. J.: A global high-resolution emission inventory for ammonia, Global Biogeochem Cycles, 11, 561–587, https://doi.org/10.1029/97GB02266, 1997.

Butler, T., Vermeylen, F., Lehmann, C. M., Likens, G. E., and Puchalski, M.: Increasing ammonia concentration trends in large regions of the USA derived from the NADP/AMoN network, Atmos. Environ., 146, 132–140, https://doi.org/10.1016/j.atmosenv.2016.06.033, 2016.

Cao, H., Henze, D. K., Shephard, M. W., Dammers, E., Cady-Pereira, K., Alvarado, M., Lonsdale, C., Luo, G., Yu, F., Zhu, L., Danielson, C. G., and Edgerton, E. S.: Inverse modeling of NH_3 sources using CrIS remote sensing measurements, Environ. Res. Lett., 15, https://doi.org/10.1088/1748-9326/abb5cc, 2020a.

Cao, H., Henze, D. K., Cady-Pereira, K., Mcdonald, B. C., Harkins, C., Sun, K., Bowman, K. W., Fu, T. M., and Nawaz, M. O.: COVID-19 Lockdowns Afford the First Satellite-Based Confirmation That Vehicles Are an Under-recognized Source of Urban NH3Pollution in Los Angeles, Environ. Sci. Technol. Lett., 9, 3–9, https://doi.org/10.1021/ACS.ESTLETT.1C00730/ASSET/IMAGES/MEDIUM/EZ1C00730_M004.GIF, 2022.

Cao, P., Lu, C., Zhang, J., and Khadilkar, A.: Northwestward cropland expansion and growing urea-based fertilizer use enhanced NH3 emission loss in the contiguous United States, Atmos. Chem. Phys., 20, 11907–11922, https://doi.org/10.5194/acp-20-11907-2020, 2020b.

Chen, Y., Shen, H., Kaiser, J., Hu, Y., Capps, S., Zhao, S., Hakami, A., Shih, J.-S., Pavur, G., Turner, M., Henze, D., Resler, J., Nenes, A., Napelenok, S., Bash, J., Fahey, K., Carmichael, G., Chai, T., Clarisse, L., Coheur, P.-F., van Damme, M., and Russell, A.: High-resolution Hybrid Inversion of IASI Ammonia Columns to Constrain U.S. Ammonia Emissions Using the CMAQ Adjoint Model, Atmos. Chem. Phys., 1–25, https://doi.org/10.5194/acp-2020-523, 2020.

Clarisse, L., Clerbaux, C., Dentener, F., Hurtmans, D., and Coheur, P.-F.: Global ammonia distribution derived from infrared satellite observations, Nat. Geosci., 2, 479–483, https://doi.org/10.1038/ngeo551, 2009.

Clarisse, L., Shephard, M. W., Dentener, F., Hurtmans, D., Cady-Pereira, K., Karagulian, F., van Damme, M., Clerbaux, C., and Coheur, P. F.: Satellite monitoring of ammonia: A case study of the San Joaquin Valley, J. Geophys. Res. Atmos., 115, 1–15, https://doi.org/10.1029/2009JD013291, 2010.

Dammers, E., Palm, M., Damme, M. van, Vigouroux, C., Smale, D., Conway, S., Toon, G. C., Jones, N., Nussbaumer, E., Warneke, T., Petri, C., Clarisse, L., Clerbaux, C., Hermans, C., Lutsch, E., Strong, K., Hannigan, J. W., Nakajima, H., Morino, I., Herrera, B., Stremme, W., Grutter, M., Schaap, M., Kruit, R. J. W., Notholt, J., Coheur, P.-F., and Erisman, J. W.: An evaluation of IASI-NH 3 with ground-based Fourier transform infrared spectroscopy measurements, Atmos. Chem. Phys, 16, 10351–10368, https://doi.org/10.5194/acp-16-10351-2016, 2016.

Dammers, E., Shephard, M. W., Palm, M., Cady-Pereira, K., Capps, S., Lutsch, E., Strong, K., Hannigan, J. W., Ortega, I., Toon, G. C., Stremme, W., Grutter, M., Jones, N., Smale, D., Siemons, J., Hrpcek, K., Tremblay, D., Schaap, M., Notholt, J., and Willem Erisman, J.: Validation of the CrIS fast physical NH3 retrieval with ground-based FTIR, Atmos. Meas. Tech., 10, 2645–2667, https://doi.org/10.5194/amt-10-2645-2017, 2017.

EPA, United States Environmental Protection Agency, Air Quality Implementation Plans, https://www.epa.gov/air-quality-implementation-plans, last access: Janauray 2023.

EPA, United States Environmental Protection Agency, Air Pollutant Emissions Trends Data, https://www.epa.gov/air-emissions-inventories/air-pollutant-emissions-trends-data, last access: August 2023.

Ellis, R. A., Jacob, D. J., Sulprizio, M. P., Zhang, L., Holmes, C. D., Schichtel, B. A., Blett, T., Porter, E., Pardo, L. H., and Lynch, J. A. Present and future nitrogen deposition to national parks in the united states: Critical load exceedances. Atmos. Chem. Phys., 13, 9083–9095. https://doi.org/10.5194/ACP-13-9083-2013, 2013

Erisman, J. W., Sutton, M. A., Galloway, J., Klimont, Z., and Winiwarter, W.: How a century of ammonia synthesis changed the world, Nat. Geosci., 1, 636–639, https://doi.org/10.1038/ngeo325, 2008.

Fehsenfeld, F. C., Huey, L. G., Leibrock, E., Dissly, R., Williams, E., Ryerson, T. B., Norton, R., Sueper, D. T., and Hartsell, B.: Results from an informal intercomparison of ammonia measurement techniques, J. Geophys. Res. Atmos., 107, https://doi.org/10.1029/2001JD001327, 2002.

Feng, J., Chan, E., and Vet, R.: Air quality in the eastern United States and Eastern Canada for 1990–2015: 25 years of change in response to emission reductions of SO_2 and NO_x in the region, Atmos. Chem. Phys., 20, 3107–3134, https://doi.org/10.5194/ACP-20-3107-2020, 2020.

Fountoukis, C. and Nenes, A.: ISORROPIAII: A computationally efficient thermodynamic equilibrium model for K^+-Ca^{2+}-Mg^{2+}-NH_4^+-Na^+-SO_4^{2-}-NO_3^--Cl^--H_2O aerosols, Atmos. Chem. Phys., 7, 4639–4659, https://doi.org/10.5194/acp-7-4639-2007, 2007.

Goldberg, D. L., Anenberg, S. C., Lu, Z., Streets, D. G., Lamsal, L. N., E McDuffie, E., and Smith, S. J.: Urban NO_x emissions around the world declined faster than anticipated between 2005 and 2019, Environ. Res. Lett., 16, 115004, https://doi.org/10.1088/1748-9326/AC2C34, 2021.

Golston, L. M., Pan, D., Sun, K., Tao, L., Zondlo, M. A., Eilerman, S. J., Peischl, J., Neuman, J. A., and Floerchinger, C.: Variability of Ammonia and Methane Emissions from Animal Feeding Operations in Northeastern Colorado, Environ. Sci. Technol., 54, 11015–11024, https://doi.org/10.1021/acs.est.0c00301, 2020.

Gu, M., Pan, Y., Sun, Q., Walters, W. W., Song, L., and Fang, Y.: Is fertilization the dominant source of ammonia in the urban atmosphere, Sci. Total Environ., 838, 155890, https://doi.org/10.1016/J.SCITOTENV.2022.155890, 2022.

Gunthe, S. S., Liu, P., Panda, U., Raj, S. S., Sharma, A., Darbyshire, E., Reyes-Villegas, E., Allan, J., Chen, Y., Wang, X., Song, S., Pöhlker, M. L., Shi, L., Wang, Y., Kommula, S. M., Liu, T., Ravikrishna, R., McFiggans, G., Mickley, L. J., Martin, S. T., Pöschl, U., Andreae, M. O., and Coe, H.: Enhanced aerosol particle growth sustained by high continental chlorine emission in India, Nat. Geosci., 14, 77–84, https://doi.org/10.1038/s41561-020-00677-x, 2021.

Guo, X., Wang, R., Pan, D., Zondlo, M. A., Clarisse, L., van Damme, M., Whitburn, S., Coheur, P. F., Clerbaux, C., Franco, B., Golston, L. M., Wendt, L., Sun, K., Tao, L., Miller, D., Mikoviny, T., Müller, M., Wisthaler, A., Tevlin, A. G., Murphy, J. G., Nowak, J. B., Roscioli, J. R., Volkamer, R., Kille, N., Neuman, J. A., Eilerman, S. J., Crawford, J. H., Yacovitch, T. I., Barrick, J. D., and Scarino, A. J.: Validation of IASI Satellite Ammonia Observations at the Pixel Scale Using In Situ Vertical Profiles, J. Geophys. Res. Atmos., 126, https://doi.org/10.1029/2020JD033475, 2021.

Hauglustaine, D. A., Balkanski, Y., and Schulz, M.: A global model simulation of present and future nitrate aerosols and their

730   direct radiative forcing of climate, Atmos. Chem. Phys., 14, 11031–11063, https://doi.org/10.5194/acp-14-11031-2014, 2014.

Hennigan, C. J., Izumi, J., Sullivan, A. P., Weber, R. J., and Nenes, A.: A critical evaluation of proxy methods used to estimate the acidity of atmospheric particles, Atmos. Chem. Phys., 15, 2775–2790, https://doi.org/10.5194/acp-15-2775-2015, 2015.

735 Hill, J., Goodkind, A., Tessum, C., Thakrar, S., Tilman, D., Polasky, S., Smith, T., Hunt, N., Mullins, K., Clark, M., and Marshall, J.: Air-quality-related health damages of maize, Nat. Sustain., 2, 397–403, https://doi.org/10.1038/s41893-019-0261-y, 2019.

Holt, J., Selin, N. E., and Solomon, S.: Changes in inorganic fine particulate matter sensitivities to precursors due to large-scale us emissions reductions, Environ Sci Technol, 49, 4834–4841, https://doi.org/10.1021/acs.est.5b00008, 2015.

740 Kendall, M.: Rank correlation methods (4th edn.) charles griffin. San Francisco, CA, 1975.

Kharol, S. K., Shephard, M. W., McLinden, C. A., Zhang, L., Sioris, C. E., O'Brien, J. M., Vet, R., Cady-Pereira, K. E., Hare, E., Siemons, J., and Krotkov, N. A.: Dry Deposition of Reactive Nitrogen From Satellite Observations of Ammonia and Nitrogen Dioxide Over North America, Geophys. Res. Lett., 45, 1157–1166, https://doi.org/10.1002/2017GL075832, 2018.

745 Lawal, A. S., Guan, X., Liu, C., Henneman, L. R. F., Vasilakos, P., Bhogineni, V., Weber, R. J., Nenes, A., and Russell, A. G.: Linked Response of Aerosol Acidity and Ammonia to SO_2 and NO_x Emissions Reductions in the United States, Environ. Sci. Technol., https://doi.org/10.1021/acs.est.8b00711, 2018.

Li, Y., Schichtel, B. A., Walker, J. T., Schwede, D. B., Chen, X., Lehmann, C. M. B., Puchalski, M. A., Gay, D. A., and Collett, J. L.: Increasing importance of deposition of reduced nitrogen in the United States, Proc. Natl. Acad. Sci. U.S.A.,

750   113, 5874–5879, https://doi.org/10.1073/pnas.1525736113, 2016.

Lindaas, J., Pollack, I. B., Garofalo, L. A., Pothier, M. A., Farmer, D. K., Kreidenweis, S. M., Campos, T. L., Flocke, F., Weinheimer, A. J., Montzka, D. D., Tyndall, G. S., Palm, B. B., Peng, Q., Thornton, J. A., Permar, W., Wielgasz, C., Hu, L., Ottmar, R. D., Restaino, J. C., Hudak, A. T., Ku, I. T., Zhou, Y., Sive, B. C., Sullivan, A., Collett, J. L., and Fischer, E. v.: Emissions of Reactive Nitrogen From Western U.S. Wildfires During Summer 2018, Journal of

755   Geophysical Research: Atmospheres, 126, https://doi.org/10.1029/2020JD032657, 2021a.

Lindaas, J., Pollack, I. B., Calahorrano, J. J., O'Dell, K., Garofalo, L. A., Pothier, M. A., Farmer, D. K., Kreidenweis, S. M., Campos, T., Flocke, F., Weinheimer, A. J., Montzka, D. D., Tyndall, G. S., Apel, E. C., Hills, A. J., Hornbrook, R. S., Palm, B. B., Peng, Q., Thornton, J. A., Permar, W., Wielgasz, C., Hu, L., Pierce, J. R., Collett, J. L., Sullivan, A. P., and Fischer, E. v.: Empirical Insights Into the Fate of Ammonia in Western U.S. Wildfire Smoke Plumes, Journal

760   of Geophysical Research: Atmospheres, 126, https://doi.org/10.1029/2020JD033730, 2021b.

Malm, W. C., Schichtel, B. A., Pitchford, M. L., Ashbaugh, L. L., and Eldred, R. A.: Spatial and monthly trends in speciated fine particle concentration in the United States, J. Geophys. Res. Atmos., 109, n/a-n/a, https://doi.org/10.1029/2003JD003739, 2004.

Miller, D. J., Sun, K., Tao, L., Pan, D., Zondlo, M. A., Nowak, J. B., Liu, Z., Diskin, G., Sachse, G., Beyersdorf, A., Ferrare, R., and Scarino, A. J.: Ammonia and methane dairy emission plumes in the San Joaquin valley of California from individual feedlot to regional scales, J. Geophys. Res. Atmos., 120, 9718–9738, https://doi.org/10.1002/2015JD023241, 2015.

McHale, M. R., Ludtke, A. S., Wetherbee, G. A., Burns, D. A., Nilles, M. A., and Finkelstein, J. S.: Trends in precipitation chemistry across the U.S. 1985–2017: Quantifying the benefits from 30 years of Clean Air Act amendment regulation, Atmos. Environ., 247, https://doi.org/10.1016/J.ATMOSENV.2021.118219, 2021.

NADP, National Atmospheric Deposition Program, the Ammonia Monitoring Network, https://nadp.slh.wisc.edu/networks/ammonia-monitoring-network/, last accessed: January 2023.

Nair, A. A. and Yu, F.: Quantification of atmospheric ammonia concentrations: A review of its measurement and modeling, https://doi.org/10.3390/atmos11101092, 1 October 2020.

Nair, A. A., Yu, F., and Luo, G.: Spatioseasonal Variations of Atmospheric Ammonia Concentrations Over the United States: Comprehensive Model-Observation Comparison, J. Geophys. Res. Atmos., 124, 6571–6582, https://doi.org/10.1029/2018JD030057, 2019.

Pan, D., Mauzerall, D. L., Benedict, K. B., Wang, R., Golston, L., Collett, J. L., Jr., Tao, L., Sun, K., Guo, X., Schichtel, B. A., Ham, J. M., Prenni, A. J., Puchalski, M., Mikoviny, T., Müller, M., Wisthaler, A., and Zondlo, M. A.: A Paradigm Shift in Sulfate-Nitrate-Ammonium Aerosol Formation in the United States and its Implications for Reactive Nitrogen Deposition, American Geophysical Union Fall Meeting 2020, Online, 1-17 Dec. 2020, A074-06, https://agu.confex.com/agu/fm20/meetingapp.cgi/Paper/679051, 2020.

Pan, D., Benedict, K. B., Golston, L. M., Wang, R., Collett, J. L., Tao, L., Sun, K., Guo, X., Ham, J., Prenni, A. J., Schichtel, B. A., Mikoviny, T., Mü, M., Wisthaler, A., and Zondlo, M. A.: Ammonia Dry Deposition in an Alpine Ecosystem Traced to Agricultural Emission Hotpots, Environ. Sci. Technol., 55, 7785, https://doi.org/10.1021/acs.est.0c05749, 2021.

Paulot, F., Jacob, D. J., Pinder, R. W., Bash, J. O., Travis, K., and Henze, D. K.: Ammonia emissions in the United States, european union, and China derived by high-resolution inversion of ammonium wet deposition data: Interpretation with a new agricultural emissions inventory (MASAGE_NH3), J. Geophys. Res. Atmos., 119, 4343–4364, https://doi.org/10.1002/2013JD021130, 2014.

Phoenix, G. K., Hicks, W. K., Cinderby, S., Kuylenstierna, J. C. I., Stock, W. D., Dentener, F. J., Giller, K. E., Austin, A. T., Lefroy, R. D. B., Gimeno, B. S., Ashmore, M. R., and Ineson, P.: Atmospheric nitrogen deposition in world biodiversity hotspots: The need for a greater global perspective in assessing N deposition impacts, Glob. Chang. Biol., 12, 470–476, https://doi.org/10.1111/j.1365-2486.2006.01104.x, 2006.

795 Pinder, R. W., Gilliland, A. B., and Dennis, R. L.: Environmental impact of atmospheric NH3 emissions under present and future conditions in the eastern United States, Geophys. Res. Lett., 35, 1–6, https://doi.org/10.1029/2008GL033732, 2008.

Puchalski, M. A., Sather, M. E., Walker, J. T., Lehmann, C. M. B., Gay, D. A., Mathew, J., and Robarge, W. P.: Passive ammonia monitoring in the United States: Comparing three different sampling devices, Journal of Environmental
800 Monitoring, 13, 3156–3167, https://doi.org/10.1039/C1EM10553A, 2011.

Puchalski, M. A., Rogers, C. M., Baumgardner, R., Mishoe, K. P., Price, G., Smith, M. J., Watkins, N., and Lehmann, C. M.: A statistical comparison of active and passive ammonia measurements collected at Clean Air Status and Trends Network (CASTNET) sites, Environ. Sci.: Process. Impacts, https://doi.org/10.1039/c4em00531g, 2015.

Schiferl, L. D., Heald, C. L., Damme, M. van, Clarisse, L., Clerbaux, C., Coheur, P., Nowak, J. B., Neuman, J. A., Herndon,
805 S. C., Roscioli, J. R., and Eilerman, S. J.: Interannual variability of ammonia concentrations over the United States : sources and implications, Atmos. Chem. Phys., 12305–12328, https://doi.org/10.5194/acp-16-12305-2016, 2016.

Shah, V., Jaeglé, L., Thornton, J. A., Lopez-Hilfiker, F. D., Lee, B. H., Schroder, J. C., Campuzano-Jost, P., Jimenez, J. L., Guo, H., Sullivan, A. P., Weber, R. J., Green, J. R., Fiddler, M. N., Bililign, S., Campos, T. L., Stell, M., Weinheimer, A. J., Montzka, D. D., and Brown, S. S.: Chemical feedbacks weaken the wintertime response of particulate sulfate
810 and nitrate to emissions reductions over the eastern United States, Proc. Natl. Acad. Sci. U.S.A., https://doi.org/10.1073/pnas.1803295115, 2018.

Sun, K., Cady-Pereira, K., Miller, D. J., Tao, L., Zondlo, M. A., Nowak, J. B., Neuman, J. A., Mikoviny, T., Müller, M., Wisthaler, A., Scarino, A. J., and Hostetler, C. A.: Validation of TES ammonia observations at the single pixel scale in the san joaquin valley during DISCOVER-AQ, J. Geophys. Res. Atmos., 120, 5140–5154,
815 https://doi.org/10.1002/2014JD022846, 2015.

Sun, K., Tao, L., Miller, D. J., Pan, D., Golston, L. M., Zondlo, M. A., Griffin, R. J., Wallace, H. W., Leong, Y. J., Yang, M. M., Zhang, Y., Mauzerall, D. L., and Zhu, T.: Vehicle Emissions as an Important Urban Ammonia Source in the United States and China, Environ. Sci. Technol., 51, 2472–2481, https://doi.org/10.1021/acs.est.6b02805, 2017.

Sun, K., Zhu, L., Cady-Pereira, K., Chan Miller, C., Chance, K., Clarisse, L., Coheur, P. F., González Abad, G., Huang, G.,
820 Liu, X., van Damme, M., Yang, K., and Zondlo, M.: A physics-based approach to oversample multi-satellite, multispecies observations to a common grid, Atmos. Meas. Tech., 11, 6679–6701, https://doi.org/10.5194/amt-11-6679-2018, 2018.

Van Damme, M., Clarisse, L., Dammers, E., Liu, X., Nowak, J. B., Clerbaux, C., Flechard, C. R., Galy-Lacaux, C., Xu, W., Neuman, J. A., Tang, Y. S., Sutton, M. A., Erisman, J. W., and Coheur, P. F.: Towards validation of ammonia (NH
825 $_3$) measurements from the IASI satellite, Atmos. Meas. Tech., 8, 1575–1591, https://doi.org/10.5194/amt-8-1575-2015, 2015.

Van Damme, M., Clarisse, L., Whitburn, S., Hadji-Lazaro, J., Hurtmans, D., Clerbaux, C., and Coheur, P. F.: Industrial and agricultural ammonia point sources exposed, Nature, 564, 99–103, https://doi.org/10.1038/s41586-018-0747-1, 2018.

Van Damme, M., Whitburn, S., Clarisse, L., Clerbaux, C., Hurtmans, D., and Coheur, P. F.: Version 2 of the IASI NH$_3$ neural network retrieval algorithm: Near-real-time and reanalysed datasets, Atmos. Meas. Tech., 10, 4905–4914, https://doi.org/10.5194/amt-10-4905-2017, 2017.

Van Damme, M., Clarisse, L., Franco, B., Sutton, M. A., Erisman, J. W., Wichink Kruit, R., van Zanten, M., Whitburn, S., Hadji-Lazaro, J., Hurtmans, D., Clerbaux, C., and Coheur, P. F. ois: Global, regional and national trends of atmospheric ammonia derived from a decadal (2008-2018) satellite record, Environ. Res. Lett., https://doi.org/10.1088/1748-9326/abd5e0, 1 May 2021.

Walker, J. M., Philip, S., Martin, R. v., and Seinfeld, J. H.: Simulation of nitrate, sulfate, and ammonium aerosols over the United States, Atmos. Chem. Phys., 12, 11213–11227, https://doi.org/10.5194/acp-12-11213-2012, 2012.

Wang, M., Kong, W., Marten, R., He, X. C., Chen, D., Pfeifer, J., Heitto, A., Kontkanen, J., Dada, L., Kürten, A., Yli-Juuti, T., Manninen, H. E., Amanatidis, S., Amorim, A., Baalbaki, R., Baccarini, A., Bell, D. M., Bertozzi, B., Bräkling, S., Brilke, S., Murillo, L. C., Chiu, R., Chu, B., de Menezes, L. P., Duplissy, J., Finkenzeller, H., Carracedo, L. G., Granzin, M., Guida, R., Hansel, A., Hofbauer, V., Krechmer, J., Lehtipalo, K., Lamkaddam, H., Lampimäki, M., Lee, C. P., Makhmutov, V., Marie, G., Mathot, S., Mauldin, R. L., Mentler, B., Müller, T., Onnela, A., Partoll, E., Petäjä, T., Philippov, M., Pospisilova, V., Ranjithkumar, A., Rissanen, M., Rörup, B., Scholz, W., Shen, J., Simon, M., Sipilä, M., Steiner, G., Stolzenburg, D., Tham, Y. J., Tomé, A., Wagner, A. C., Wang, D. S., Wang, Y., Weber, S. K., Winkler, P. M., Wlasits, P. J., Wu, Y., Xiao, M., Ye, Q., Zauner-Wieczorek, M., Zhou, X., Volkamer, R., Riipinen, I., Dommen, J., Curtius, J., Baltensperger, U., Kulmala, M., Worsnop, D. R., Kirkby, J., Seinfeld, J. H., El-Haddad, I., Flagan, R. C., and Donahue, N. M.: Rapid growth of new atmospheric particles by nitric acid and ammonia condensation, Nature, 581, 184–189, https://doi.org/10.1038/s41586-020-2270-4, 2020.

Wang, R., Guo, X., Pan, D., Kelly, J. T., Bash, J. O., Sun, K., Paulot, F., Clarisse, L., van Damme, M., Whitburn, S., Coheur, P. F., Clerbaux, C., and Zondlo, M. A.: Monthly Patterns of Ammonia Over the Contiguous United States at 2-km Resolution, Geophys. Res. Lett., 48, https://doi.org/10.1029/2020GL090579, 2021.

Warner, J. X., Wei, Z., Larrabee Strow, L., Dickerson, R. R., and Nowak, J. B.: The global tropospheric ammonia distribution as seen in the 13-year AIRS measurement record, Atmos. Chem. Phys., 16, 5467–5479, https://doi.org/10.5194/acp-16-5467-2016, 2016.

Warner, J. X., Dickerson, R. R., Wei, Z., Strow, L. L., Wang, Y., and Liang, Q.: Increased atmospheric ammonia over the world's major agricultural areas detected from space, Geophys. Res. Lett., 44, 2875–2884, https://doi.org/10.1002/2016GL072305, 2017.

Whitburn, S., van Damme, M., Clarisse, L., Bauduin, S., Heald, C. L., Hadji-Lazaro, J., Hurtmans, D., Zondlo, M. A., Clerbaux, C., and Coheur, P.-F.: A flexible and robust neural network IASI-NH 3 retrieval algorithm, J. Geophys. Res. Atmos., 121, 6581–6599, https://doi.org/10.1002/2016JD024828, 2016.

Yao, X. and Zhang, L.: Trends in atmospheric ammonia at urban, rural, and remote sites across North America, Atmos. Chem. Phys., 16, 11465–11475, https://doi.org/10.5194/acp-16-11465-2016, 2016.

Yao, X. and Zhang, L.: Causes of Large Increases in Atmospheric Ammonia in the Last Decade across North America, ACS Omega, 4, 22133–22142, https://doi.org/10.1021/acsomega.9b03284, 2019.

865 Yu, F., Nair, A. A., and Luo, G.: Long-Term Trend of Gaseous Ammonia Over the United States: Modeling and Comparison With Observations, J. Geophys. Res. Atmos., 123, 8315–8325, https://doi.org/10.1029/2018JD028412, 2018.

Yue, S. and Wang, C. Y.: The Mann-Kendall test modified by effective sample size to detect trend in serially correlated hydrological series, Water Resources Management, https://doi.org/10.1023/B:WARM.0000043140.61082.60, 2004.

Zhai, S., Jacob, D. J., Wang, X., Liu, Z., Wen, T., Shah, V., Li, K., Moch, J. M., Bates, K. H., Song, S., Shen, L., Zhang, Y.,
870 Luo, G., Yu, F., Sun, Y., Wang, L., Qi, M., Tao, J., Gui, K., Xu, H., Zhang, Q., Zhao, T., Wang, Y., Lee, H. C., Choi, H., and Liao, H.: Control of particulate nitrate air pollution in China, Nat. Geosci., 14, 389–395, https://doi.org/10.1038/s41561-021-00726-z, 2021.

Zheng, G., Su, H., Wang, S., Andreae, M. O., Pöschl, U., and Cheng, Y.: Multiphase buffer theory explains contrasts in atmospheric aerosol acidity, Science (1979), 369, 1374–1377, https://doi.org/10.1126/SCIENCE.ABA3719, 2020.

875